1965

Photodielectric effect in semiconductors

Norman Gregg Dillman
Iowa State University

66–2984

DILLMAN, Norman Gregg, 1938–
PHOTODIELECTRIC EFFECT IN SEMI-CONDUCTORS.

Iowa State University of Science and Technology
Ph.D., 1965
Engineering, electrical

University Microfilms, Inc., Ann Arbor, Michigan

PHOTODIELECTRIC EFFECT IN SEMICONDUCTORS

by

Norman Gregg Dillman

A Dissertation Submitted to the

Graduate Faculty in Partial Fulfillment of

The Requirements for the Degree of

DOCTOR OF PHILOSOPHY

Major Subject: Electrical Engineering

Approved:

Signature was redacted for privacy.

In Charge of Major Work

Signature was redacted for privacy.

Head of Major Department

Signature was redacted for privacy.

Dean of Graduate College

Iowa State University
Of Science and Technology
Ames, Iowa

1965

TABLE OF CONTENTS

LIST OF FIGURES

LIST OF TABLES

INTRODUCTION

The absorption of light by a solid causes electrons within the solid to assume higher energy levels. This process gives rise to phenomena such as photoconductivity, photovoltaic effect, Dember effect, photomagneto-electric effect (PME) and the photodielectric effect.

The history of photoeffects is well documented by Bube (3) and begins in 1873 when Willoughby Smith observed and recorded that the conductivity of resistors made of bars of high resistivity selenium increased from 15 to 20 percent when exposed to light. Most of the early work was concentrated on cataloging materials exhibiting photoconductivity and the other photoeffects. With the discovery of the Dember effect (or crystal photoeffect as it was called) and the photomagnetoelectric effect in the 1920s all of the basic photoeffects were known. Prior to World War II very little had been written to explain these phenomena in terms of traps, recombination centers, carrier lifetimes and transit times. Gudden, Pohl and a few others were the pioneers of modern photoconductivity in the 1920s, but it was not until the 1950s that many papers were published expressing present day concepts (3, 21, 24, 25, 26).

The purpose of this dissertation is to examine the mechanisms giving rise to the photodielectric effect. This includes a review of the various hypotheses developed by other investigators, the formulation of mathematical models showing the relationship between these hypotheses and the terminal characteristics of a photocapacitor, and the presentation of pertinent experimental data obtained from observations upon CdS single crystals.

Photoeffects

Many of the photoeffects mentioned in the introductory paragraph may be present concurrently in any particular experimental situation, and since the presence of more than one photoeffect could influence the interpretation of the data, it is desirable to present a brief survey of all of the aforementioned photoeffects.

Photodielectric effect

The term photodielectric effect refers to the change in capacitance that is observed when the dielectric of a capacitor is illuminated. This effect was first observed in 1909 by Lenard and Saeland, and was investigated more intensively by Gudden and Pohl in the 1920s. References to later investigations may be found in review papers by Garlick (7) and Bube (3). To date most work has been with polycrystalline or powdered materials because of the difficulty in obtaining large single-crystals of many compounds. This is one of the reasons for the relatively slow development of a complete theoretical treatment of photoeffects.

There are basically three hypotheses to explain the photodielectric effect, 1) trapped electrons, 2) nonuniform illumination and 3) spacecharge at grain boundaries.

Trapped electrons Some of the electrons generated by illumination are captured by the traps near the conduction band. Since these are less tightly bound than electrons in valence bands, they could conceivably have abnormally high polarizabilities. Consequently, the permittivity of the material would be increased if a significant number of traps were occupied

by the optically-generated electrons.

Garlick and Gibson (9) used this hypothesis to explain a 75 percent increase in capacitance for ZnS powders. They associated the photocapacitance with the traps because, (a) the temperature dependence of the capacitance and the density of electrons in traps were both exponential, (b) transient variation of phosphorescence was much faster than the emptying of the traps or the variation of capacitance, (c) the traps were filled and the photocapacitance saturated at a relatively low light intensity and (d) the relaxation time determined from frequency response measurements corresponded to a loosely bound electron in a trap. In another paper Garlick and Gibson (8) noted two relaxation times for the phosphor $CaWO_4$-U with two activators indicating that the photocapacitance was due to the traps.

Nonuniform illumination If a material absorbs illumination strongly, the light intensity will decrease exponentially with distance from the illuminated surface. This means that the material near the surface will be more conductive than the rest of the material, thus effectively decreasing the thickness of the insulating region. This causes the capacitance to increase.

Kallmann et. al. (16) used this hypothesis to interpret the results of their observations on (ZnCd)S luminescent powders. They assumed that the material could be divided into two regions, one insulating and one photosensitive. The total impedance of the material was found by adding the impedance of the two regions. The impedance of the photosensitive region was calculated by assuming that the conductivity varied linearly

with light intensity and integrating. It is noteworthy that the assumption of Garlick and Gibson, i.e. that polarizable traps are significant, was not necessary to explain the increase in capacitance in the material used by Kallmann.

In a later work, Kallmann et. al. (15) measured increases in capacitance ranging from 2 to nearly 10^6 times for single-crystal CdS with transparent gold contacts. They concluded that such a large increase could not be due to polarization of electrons in traps and presented evidence to support their hypothesis that the photodielectric effect is primarily due to the photoconductivity causing an apparent decrease in thickness of the material. Kronenberg and Accardo (19) concluded from impedance measurements of ZnS and CdS type powders that both trapped electrons and the photoconductive reduction of the thickness are necessary to adequately explain the change of capacitance.

Kallmann et. al. (14, 15, 16) have offered explanations for the photodielectric effect in a heterogeneous material such as a luminescent powder based on uniform illumination and no change in permittivity. A typical model for such a system consists of two layers, one an insulating layer due to the material that binds the luminescent powders together and another layer to account for the photosensitive material. The first layer is represented by a fixed capacitor which is in series with a parallel resistor and capacitor representing the photosensitive layer. Usually the resistor is the only component that varies with light intensity meaning that the photodielectric effect is due to the nonuniformity in photoconduction and not a result of a real change in the permittivity of the material. This

technique is useful in determining the photoconductivity of a material from powders when large single-crystals are not available (14).

Space charge at grain boundaries. The third hypothesis applies only to polycrystalline materials and will not be considered after this section. In 1955 after publishing several papers explaining the photodielectric effect in luminescent powders by the trapped electron hypothesis, Garlick (6) measured only a small change in capacitance for single-crystals of ZnS and CdS and concluded that the photodielectric effect in powders was probably due to grain boundary dipole layers.

Further explanations have been offered by Mark and Kallmann (20). They applied the Maxwell-Wagner theory and the method of the Cole-Cole diagram to analyse a.c. impedance measurements of crystalline powdered ZnCdS photoconductors. They concluded that the photodielectric effect is due to the finite mobility of "free" charges in photoconducting regions of the photocapacitor. At low frequencies the charges move to the surface of the photoconducting regions and contribute to the polarization of the material. At higher frequencies the free charges move too slowly to follow the a.c. field and the result is a relaxation phenomenon. The polarization at low frequencies is proportional to the number of free carriers and the result is the photodielectric effect. The photodielectric effect in wafers of doped germanium single-crystals has also been attributed to the drift of minority carriers generated by illumination (22).

A few devices utilizing the photodielectric effect have been constructed and analyzed. Gordon, et al. (11) made a photocapacitor of CdS powders imbedded in plastic. Saturation was noted when the photocapitance

reached approximately 1.6 its original value. It was proposed that the capacitor be used in a resonant circuit to increase the sensitivity. The device is useful only when slow response times are acceptable. Sihvonen, et al. (28) designed and tested a two-layer photocapacitor with an active layer of CdS and an inactive layer of either $BaTiO_3$ or silicone plastic. At low light intensities, the active material appears as an insulator and the equivalent permittivity of the device approaches

$$\varepsilon = \frac{\varepsilon_1\varepsilon_2(d_1 + d_2)}{\varepsilon_1 d_2 + \varepsilon_2 d_1} \tag{1}$$

where ε is the permittivity, and d is the thickness. The subscript 1 refers to the inert material and 2 refers to the active material. At higher light intensities, the active region acts like a short circuit and the permittivity approaches that of the passive region. Sihvonen, et al. analyzed the two layer system in terms of both the permittivity and the dielectric loss factor of each region. An increase in capacitance of 2500 times was obtained with the $BaTiO_3$ passive region for frequencies up to 0.22 Mcs. and a capacitance increase of 20 times for the silicone plastic/CdS device for frequencies up to about 10 Mcs. Applications for such a device are limited by its frequency response as noted and also by its slow response to light changes. The dissipation factor is also significant under certain conditions.

Conductivity and photoconductivity

The conductivity may be derived in terms of material parameters by starting with a basic definition of current.

$$I = (Q_+/T_{r+}) + (Q_-/T_{r-}) \tag{2}$$

where Q_+ is the total charge associated with free holes, Q_- is the total charge associated with free electrons, and T_r is the time required for a carrier to move from one contact to the other. If the current is all due to absorption of radiation (insulator in the dark), then

$$Q_+ = eF\tau_p \text{ and } Q_- = eF\tau_n \tag{3}$$

where e is the charge on an electron, F is the rate at which electron-hole pairs are generated by absorption and τ_p and τ_n are the lifetimes of free holes and electrons respectively. Then

$$I = eF(\tau_p/T_{r+} + \tau_n/T_{r-}). \tag{4}$$

The term containing the ratio of lifetime to transit time is called the photoconductive gain and is equal to the number of carriers passing through the material per absorbed photon of light. Under certain conditions the photoconductive gain can be greater than one.

Substituting for the transit times and solving for the d.c. conductance, G yields

$$G = \frac{eF}{L^2}(\tau_p\mu_p + \tau_n\mu_n)$$

where μ is the mobility and L is the length of material. If f is the rate of generation per unit volume, then the conductivity is

$$\sigma = ef(\tau_p\mu_p + \tau_n\mu_n). \tag{5}$$

Note that the concentration of free holes is

$$p = f\tau_p \tag{6}$$

and the concentration of free electrons is

$$n = f\tau_n. \tag{7}$$

Substituting these expressions into Equation 5 yields the familiar equation for conductivity,

$$\sigma = e(p\mu_p + n\mu_n). \tag{8}$$

The variation of conductivity with light intensity depends on the nature of the traps, recombination centers and the level of absorbed radiation (2, 3, 13, 24, 25, 26, 30). The conductivity of an insulator may be represented as a power of the light intensity,

$$\sigma \propto \phi^{\beta}. \tag{9}$$

The parameter β is usually constant but can vary slowly with light intensity. Typically β will be unity at low intensities, will change to 1/2 for several decades of increasing light intensity and will finally return to unity again. It is also possible for β to be greater than unity for a limited range of intensities (e.g. 3 to 5). This is called supralinearity and has been explained in terms of recombination centers acting as traps with increasing light intensity (25).

The following is a summary of conditions that determine the various

values for β:

$\sigma \propto (\phi)^{\frac{1}{2}}$ The conductivity will vary as the square root of light intensity for an ideal trap-free material (3, 24). It will also vary in this manner in a material containing traps if the density of occupied traps above the electron Fermi level is greater than the density of those below the Fermi level (25).

$\sigma \propto (\phi)^{\beta}$ $(\frac{1}{2} < \beta < 1)$ If the Fermi level is in the midst of an exponential distribution of traps, the conductivity will vary as a fractional power of light intensity between 1/2 and 1 (3, 24, 25).

$\sigma \propto (\phi)$ The variation will be linear if the distribution of traps is linear.

$\sigma \propto (\phi)^{\beta}$ $(1 < \beta)$ As noted previously, this condition is called supralinearity. Rose (25) ascribes supralinearity to two distinct defect states in the forbidden zone with different capture cross-sections. One set (called class I) is near the center of the band. These states act as recombination centers. The second set of states (class II) is outside both Fermi levels for low light intensities, therefore, these act as traps. With increasing light intensity, the Fermi levels move out through these states and they become recombination centers. The lifetime of electrons increases continuously during the transition period causing the greater increase in the conductivity.

Another factor tending to produce an increasing conductivity is the dependence of the carrier mobility on the number of occupied traps (17, 18,

31, 32). As the light intensity increases, the number of traps remaining to capture carriers decreases with a corresponding increase in the mobility. Thus,

$$\mu_t = \mu \frac{n}{n + n_t} . \qquad (10)$$

In the above equation μ_t is the effective mobility, μ is the trap free mobility, n is the density of free carriers and n_t is the density of trapped carriers. If $n << n_t$, then μ_t is smaller than μ. If $n > n_t$, then μ_t is approximately equal to μ.

Photovoltaic effects

Photovoltaic effects are characterized by a voltage or potential difference across a material that is absorbing radiation. A potential barrier in the vicinity of the absorbed radiation is necessary. The potential barrier may be caused by 1) a p-n junction, 2) a metal-to-semiconductor junction, 3) a difference between the surface conductivity and the volume conductivity of a material, and 4) a junction of two semiconducting materials with different band gaps. The simple energy diagram for a p-n junction in Figure 1 will be used to explain the voltage that appears across an illuminated junction. Electron-hole pairs are generated when the material is illuminated by light with a frequency equal to or greater than a critical frequency determined by the band gap of the material. The critical frequency f and the band gap E_g are related by

$$E_g = hf \qquad (11)$$

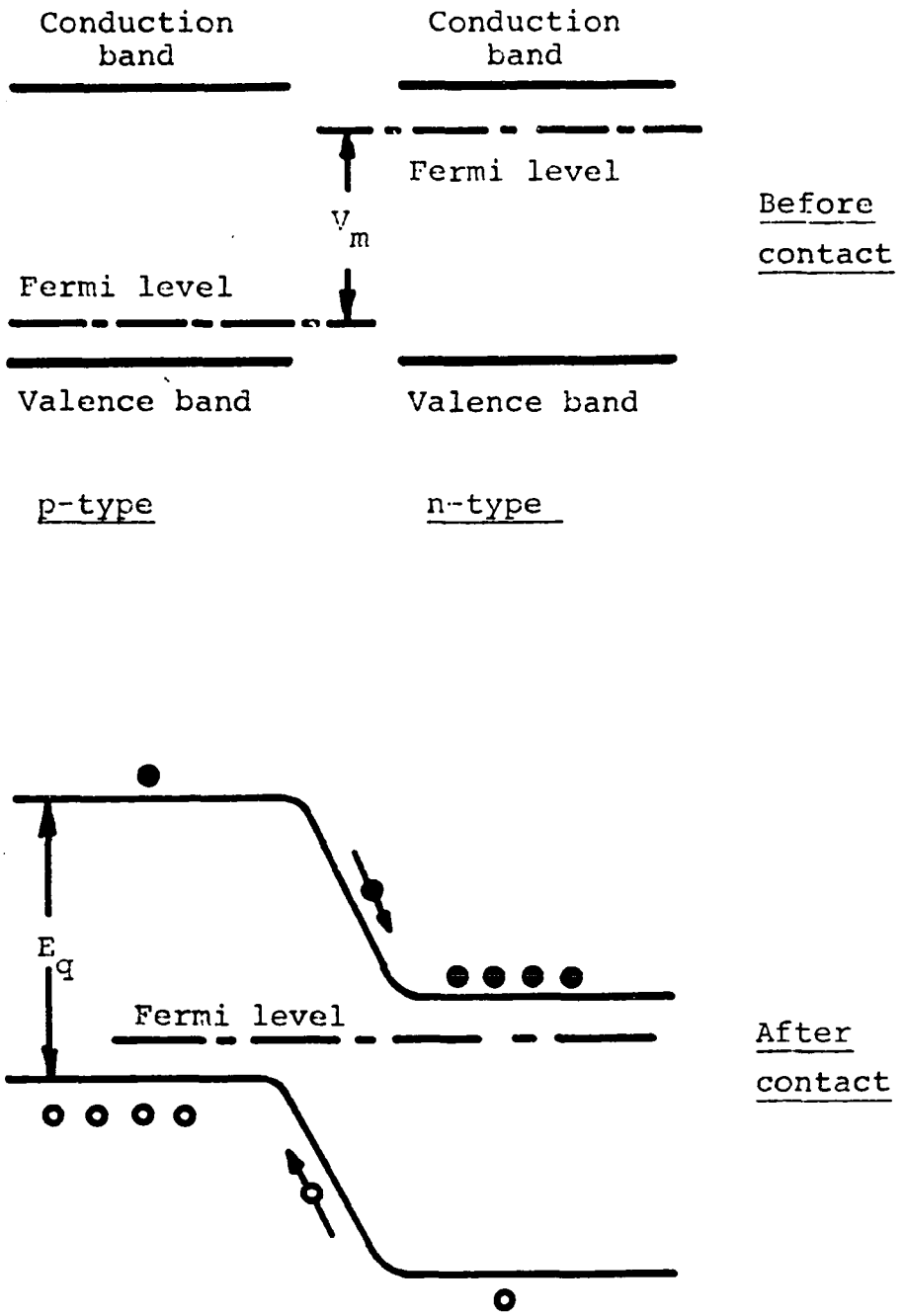

Figure 1. Energy diagram for a p-n junction

where h is Planck's constant. If the p and n regions are connected through a short circuit, a current will flow when the junction is illuminated. The current is due to minority carriers flowing across the junction, i.e. electrons flowing from the p to the n region and holes flowing from the n to the p region. If the terminals are open-circuited, a voltage will build up across the junction to balance the flow of minority carriers. The open-circuit voltage approaches a maximum of V_m, the difference in the Fermi levels of the two materials which is always less than the band gap. The Dember and photomagnetoelectric effects could also be classified as photovoltaic effects but will be discussed separately.

The Dember effect If a material has different electron and hole mobilities, a voltage gradient will exist in the direction of strongly absorbed radiation. This is known as the Dember effect. The concentration of holes and electrons varies with position when the radiation is greatly attenuated or strongly absorbed. The holes and electrons tend to diffuse into the region of lower concentration. When the lifetime of one type of the carrier differs from the other, there will be an electric field in the direction of the radiation resulting from the unequal charge distribution.

The photomagnetoelectric (PME) effect If the same conditions exist as for the Dember effect but, in addition, a magnetic field is applied perpendicular to the radiation, then an electric field is produced which is perpendicular to both the radiation and the magnetic field. This is called the photomagnetoelectric effect and is equivalent to the Hall effect except the current is produced by the diffusion of the generated

electron-hole pairs from the region of high concentration. It is not necessary that the mobilities of the carriers be different for the photomagnetoelectric effect because the potential difference is due to the deflection of the hole and electron diffusion currents in opposite directions by the magnetic field.

MATHEMATICAL MODELS

The models that are constructed and analyzed in this section are designed to show the relative importance of the hypotheses discussed in the introduction. It is important to note that agreement between experimental data and the results of the analysis of a model indicates that the model is a possible explanation or representation of actual physical processes, but it does not necessarily prove that the model is the only explanation or representation of the actual physical processes involved.

The models to be analyzed all relate to the photocapacitor in Figure 2. Light is incident normal to a semitransparent contact and inside the dielectric, the light intensity, the conductivity, and the permittivity all vary with respect to a position-coordinate normal to the illuminated surface. The basic analytical problem is to relate the spatial variation of permittivity and conductivity to the admittance of the capacitor. The results of the analysis are a comparison of the real and the imaginary parts of the a.c. admittance as the light intensity, photosensitivity, frequency and other parameters vary. Optical density measurements are not required to compare the models with experimental results. This is an advantage because the problems associated with optical density measurements such as absorption and reflection of light at the electrical contacts are avoided.

The a.c. admittance of a two-terminal device may be defined as the ratio of the phasor representing the a.c. current flowing through the device to the phasor representing the a.c. voltage across the terminals. The real part of the a.c. admittance is the parallel conductivity G, and

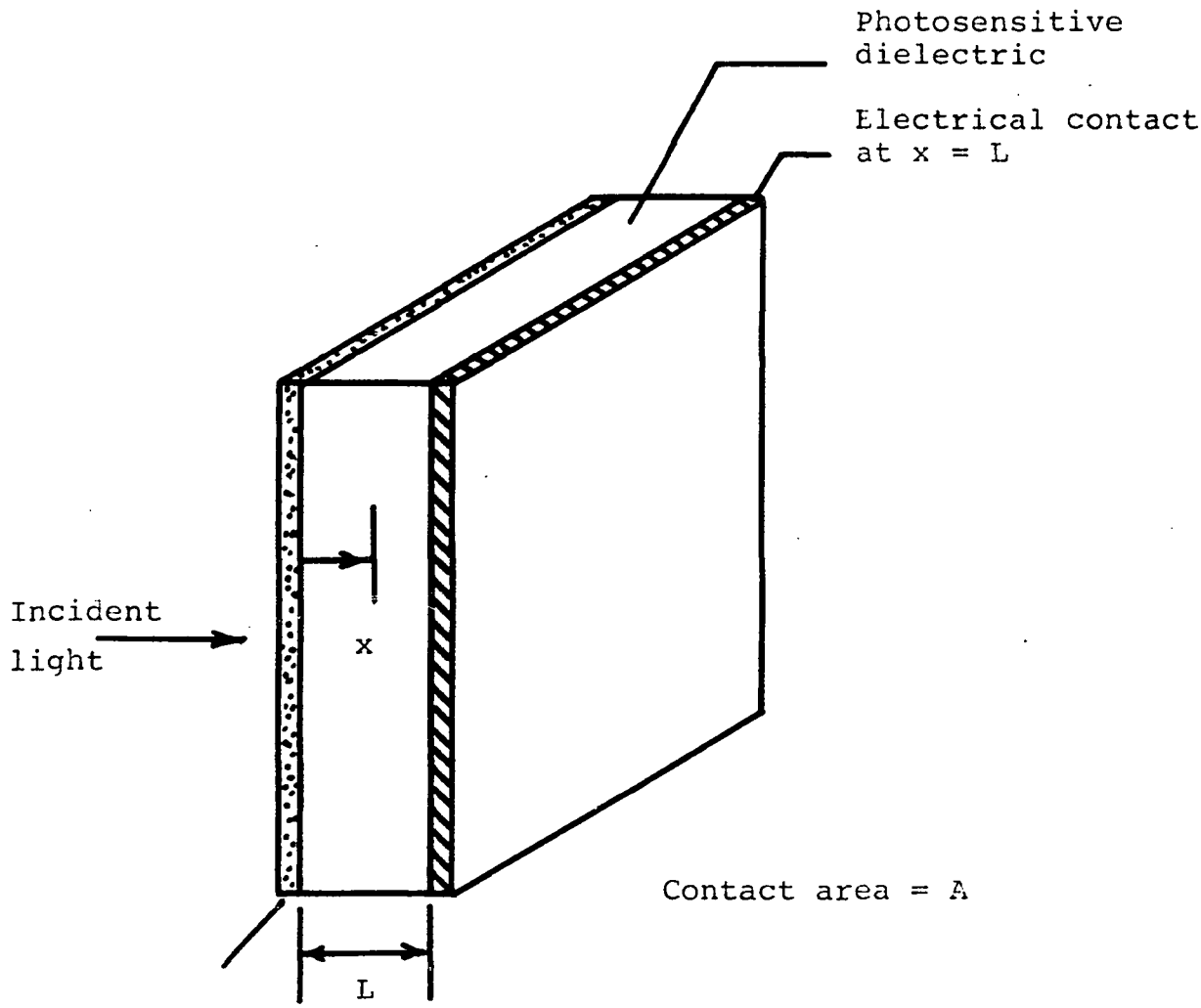

Figure 2. Drawing of a photocapacitor, i.e., a capacitor with a photosensitive dielectric. Not drawn to scale

the imaginary part is the susceptance B, i.e.,

$$Y = G + jB. \tag{12}$$

For the device shown in Figure 2, the equivalent conductivity of the dielectric material is

$$\sigma_{eq} = GL/A \tag{13}$$

where A is the area of the cross-section and L is the thickness. The equivalent permittivity ε_{eq} is

$$\varepsilon_{eq} = CL/A \tag{14}$$

where C is the equivalent parallel capacitance defined as

$$C = B/2\pi f, \quad (f = \text{frequency}). \tag{15}$$

The following equation defines a normalized admittance y that does not depend on the thickness or the area of the dielectric material:

$$y = YL/A = \sigma_{eq} + j\omega\varepsilon_{eq}. \tag{16}$$

The normalized admittance is related to the permittivity and the conductivity by

$$y = \left[\frac{1}{L}\int_{o}^{L} \frac{dx}{\sigma(x) + j\omega\varepsilon(x)}\right]^{-1} \tag{17}$$

where the symbols are defined in Table 1. If the conductivity and the permittivity are not functions of position, the normalized admittance

Table 1. Definitions of symbols relating to the models and Figure 2

x	= distance from the illuminated surface
L	= thickness of the material
A	= contact area
$\gamma = \alpha L$	= number of absorption thicknesses
α	= absorption coefficient
$\phi = \phi(x)$	= light intensity (may or may not be a function of position)
$\phi_o = \phi^+(o^+)$	= light intensity at $x = o^+$ with positive x propagation
$\sigma = \sigma(x)$	= conductivity (may or may not be a function of position)
σ_o	= "dark" conductivity
$\sigma_\rho = P_\sigma \phi^\beta$	= photoconductivity
$\sigma(x)$	= $\sigma_o + \sigma_\rho$
p_σ	= photoconductivity constant
ε	= dielectric constant or permittivity
ε_o	= dielectric constant of free space
ε_r	= relative dielectric constant (with no illumination)
$\varepsilon_p = p_\varepsilon \phi$	= photodielectric term
ε	= $\varepsilon_o \varepsilon_r + \varepsilon_\rho$
p_ε	= photodielectric sensitivity
C_o	= dark capacitance
$f = \omega/2\pi$	= frequency of the applied sinusoidal voltage
j	= $\sqrt{-1}$

reduces to

$$y = \sigma + j\omega\varepsilon = \sigma_{eq} + j\omega\varepsilon_{eq}. \tag{18}$$

The models are divided into two groups. Group A includes all models in which either conductivity or permittivity vary with position. Under these circumstances, Equation 17 must be used to determine the normalized admittance. For homogeneous materials, it is assumed that the variation is due to a change in light intensity in the x-direction. Group B consists of models in which the light intensity is constant inside the material so the conductivity and permittivity do not vary with position. For group B models, the variation of conductivity and permittivity with light intensity is the only information required to solve for the normalized admittance by Equation 18.

The variation of conductivity with light intensity is discussed in the introduction. The salient points that were developed there are, 1) the parameter β characterizes the variation of the conductivity with light intensity according to the equation

$$\sigma \propto \phi^{\beta} \tag{9}$$

and 2) β may have values varying upward from 1/2 depending on the light intensity and the distribution of traps and recombination centers. Values of β equal to 1/2, 1 and 2 are selected for the models in group B and 1 and 2 for group A.

For both models, the permittivity is assumed to vary linearly with light intensity. This is justified by assuming the hypothesis that the increase is due to electrons captured in traps. If the traps are not

filled, i.e., saturated, the number of occupied traps is proportional to the rate of optical generation or light intensity. According to this assumption then, the permittivity and the light intensity at a point inside the dielectric are related by

$$\varepsilon = \varepsilon_o \varepsilon_r + p_\varepsilon \phi. \tag{19}$$

To solve for the normalized admittance using Equation 17 (group A), the variation of light intensity with position must be known in addition to the variation of conductivity and permittivity with light intensity just discussed. In other words, by combining the equations that define the variation of conductivity and permittivity with light intensity, and light intensity with position, the variation of conductivity and of permittivity with position may be determined.

The light intensity within the dielectric may be divided into two parts. In Equation 20, $\phi^+(x)$ is the intensity of the light traveling in the positive x direction and $\phi^-(x)$ is the intensity of the light traveling the negative x direction. Thus, the total light intensity at a point is

$$\phi = \phi(x) = \phi^+(x) + \phi^-(x). \tag{20}$$

It is assumed that the light intensity in the negative x direction is due to reflection of light at x = L. To further simplify the problem, it is assumed that the light traveling in the negative x direction will not be reflected from the surface at x = o. Using Beer's law and assuming total reflection at the back surface, the two components of light intensity are

$$\phi^+(x) = \phi_o e^{-\alpha x} \text{ and } \phi^-(x) = (\phi_o e^{-\alpha L})(e^{\alpha(x-L)}) \tag{21}$$

where $\phi_o = \phi^+(o^+)$ is the intensity of the light transmitted through the front surface as measured at $x = o^+$. The constant α is the absorption coefficient. For the case of no reflection at $x = L$, the light intensity as a function of position is

$$\phi = \phi(x) = \phi_o e^{-\alpha x} \tag{22}$$

and for the case of total reflection at the back contact, it is

$$\phi = \phi(x) = 2(\phi_o)(e^{-\alpha L})\cosh[\alpha(x-L)]. \tag{23}$$

The following outlines the development of the mathematical models of the photodielectric effect in a single-crystal photocapacitor: 1) Either Equation 22 or 23 is used to specify the variation of light intensity with position for the models in group A. The light intensity is uniform throughout the dielectric for group B models. 2) The results of step 1 are substituted into Equations 9 and 19 which then specify the variation of conductivity and permittivity with position. 3) For group A, the results of step 2 are substituted into the equation for the normalized admittance (Equation 17) and the indicated integration is carried out. Equation 18 is used to determine the normalized admittance for group B and integration is not required. 4) The final step is the evaluation of the real and imaginary parts of the normalized admittance for specific values or sets of values of the following parameters which are defined in Table 1: γ, ϕ_o, σ_o, p_σ, ε_o, ε_r, p_ε and f.

Table 2 summarizes the parameters which differentiate the various models. The variation of the remaining parameters is given with the

Table 2. Summary of the parameters specifying the models

Group A - Nonuniform Illumination			$\sigma_o = 0$ $\varepsilon_r = 10$	
Model number	1	2	3	4
Variation of conductivity with light, $\sigma \propto \phi^{\beta}$	$\beta = 1$	$\beta = 1$	$\beta = 1$	$\beta = 2$
Variation of permittivity with light, $\varepsilon = \varepsilon_o\varepsilon_r + p_\varepsilon\phi$	$p_\varepsilon \doteq 0$	$p_\varepsilon \neq 0$	$p_\varepsilon = 0$ and $p_\varepsilon \neq 0$	$p_\varepsilon = 0$ and $p_\varepsilon \neq 0$
Reflection from back contact	yes $\bar{\phi} \neq 0$	yes $\bar{\phi} \neq 0$	no $\bar{\phi} = 0$	no $\bar{\phi} = 0$

Group B - Uniform Illumination			$\sigma_o = 0$ $\varepsilon_r = 10$
Model number	1	2	3
Variation of conductivity with light, $\sigma \propto \phi^{\beta}$	$\beta = 1/2$	$\beta = 1$	$\beta = 2$
Variation of permittivity with light, $\varepsilon = \varepsilon_o\varepsilon_r + p_\varepsilon\phi$	$p_\varepsilon \neq 0$	$p_\varepsilon \neq 0$	$p_\varepsilon \neq 0$

results which are plotted in Figures 3 through 10.

In the remainder of this section, the equations for the models will be derived and the results of the computations will be presented. The models were selected to represent a wide range of possible material parameters. For a given photocapacitor the model parameters such as γ, p_ε/p_o and β could be adjusted to obtain the best correlation between the photocapacitor data and the model. Digital computer programs have been written that will determine the parameters giving the least-mean-square-error between model 4 of group A and experimental results. For group B, the digital computer is not required to obtain the least-mean-square-error fit. Such a fit is derived in the last section.

Group A - Model 1

Model 1 demonstrates the second hypothesis discussed in the introduction; that is, the equivalent capacitance may change with light intensity even though the permittivity is insensitive to light ($p_\varepsilon = o$). The following additional specifications are made for this model: 1) $\beta = 1$ and 2) all of the light is reflected at the back contact. Equations 9, 19 and 20 may be written as

$$\sigma = \sigma_o + p_\sigma \phi,$$

$$\varepsilon = \varepsilon_o \varepsilon_r$$

and $$\phi = 2\phi_o e^{-\alpha L} \cosh[\alpha(x-L)].$$

Substituting the last three equations into Equation 17 yields

$$\frac{1}{y} = \frac{1}{L}\int_{o}^{L} \frac{dx}{(\sigma_o + j\omega\varepsilon_o\varepsilon_r) + p_\sigma 2\phi_o e^{-\gamma}\cosh[\alpha(x-L)]}. \tag{24}$$

To simplify notation, let $y_o = \sigma_o + j\omega\varepsilon_o\varepsilon_r$, (25)

$$y_i = p_\sigma 2\phi_o e^{-\gamma}, \tag{26}$$

and $x' = \alpha(x-L)$. (27)

Then, $$\frac{1}{y} = \frac{1}{\alpha L}\int_{-\gamma}^{o} \frac{dx'}{y_o + y_i\cosh(x')}. \tag{28}$$

Integrating and then inverting yields

$$y = \frac{\gamma(y_o - y_i)^{\frac{1}{2}}(y_o + y_i)^{\frac{1}{2}}}{\ln \dfrac{(y_o - y_i)^{\frac{1}{2}} + (y_o - y_i)^{\frac{1}{2}}\tanh(\gamma/2)}{(y_o + y_i)^{\frac{1}{2}} - (y_o - y_i)^{\frac{1}{2}}\tanh(\gamma/2)}} \tag{29}$$

where y_o and y_i are defined by Equations 25 and 26. The real and imaginary parts of the normalized admittance y are characterized by the normalized photocapacitance C/C_o and the equivalent conductivity σ_{eq}, where

$$C/C_o = (\text{imaginary part of } y)/\varepsilon_o\varepsilon_r\omega = \varepsilon_{eq}/\varepsilon_o\varepsilon_r, \tag{30}$$

and $$\sigma_{eq} = (\text{real part of } y). \tag{31}$$

The normalized photocapacitance and the equivalent conductivity were computed on the Cyclone digital computer at Iowa State University using the relative dielectric constant for CdS (approximately 10) with the "dark" conductivity set equal to zero. Various values for the number of absorption thicknesses, for the frequency, and for the light intensity at the surface of the material were used in the digital computer program to obtain the curves plotted in Figures 3 through 8. The significance of these curves will be discussed in the last section. The same procedure was used to obtain the results for the other models in group A. The digital computer programs used are discussed in the appendix.

Group A - Model 2

Model 2 is the same as model 1 except the permittivity is now considered to vary with light intensity, i.e., p_ε is no longer zero. If y_i is redefined for model 2 as

$$y_i = y_i' = (p_\sigma + j\omega p_\varepsilon)2\phi_o e^{-\gamma} \tag{32}$$

then Equation 29 is the solution for both model 1 and model 2. The digital computer results for model 2 are plotted with some of the results of model 1 for comparison in Figure 7. The addition of a variation of permittivity with light intensity causes an increased photocapacitive effect. If the sensitivity of the permittivity to light increases, the increase in capacitance becomes significant at lower conductivities.

Group A - Model 3

The purpose of model 3 is to show how the results of model 1 would change if reflection at the contact at x = L were neglected, i.e., $\bar{\phi}(x) = o$. The assumption of no reflection at the back contact greatly simplifies the derivation of the expression for the normalized admittance for model 4. If the same conditions used for model 1 are substituted into Equation 17 with the exception that

$$\phi = \phi_o e^{-\alpha x},$$

then the normalized admittance for model 3 becomes

$$y = \frac{\gamma y_o}{\ln \dfrac{e^{\gamma} y_o + y_i''}{y_o + y_i''}} \tag{33}$$

where

$$y_i'' = (p_\sigma + j\omega p_\varepsilon)\phi_o. \tag{34}$$

The assumption of no reflection at the back contact is not true for the photocapacitor, but the results plotted in Figure 8 indicate that for low and moderate light intensities, reflection from the back surface has a negligible effect.

Group A - Model 4

Model 4 represents supralinear variation of the conductivity with light intensity. One example is selected with $\beta = 2$. Therefore,

$$\sigma = p_\sigma(\phi)^2 \tag{35}$$

and $$\varepsilon = \varepsilon_o\varepsilon_r + p_\varepsilon\phi. \tag{19}$$

The results of model 3 indicate, even for a reflecting back contact, the light intensity may be approximated as

$$\phi = \phi_o(e^{-\alpha x}). \tag{22}$$

Then Equation 17 may be written as

$$\frac{1}{y} = \frac{1}{L}\int_o^L \frac{dx}{p_\sigma\phi^2 + j\omega p_\varepsilon\phi + j\omega\varepsilon_o\varepsilon_r},$$

but

$$\frac{\delta\phi}{\delta x} = -(\alpha\phi),$$

so

$$\frac{1}{y} = \frac{-1}{\alpha L}\int_{\phi_i}^{\phi_i e^{-\gamma}} \frac{d\phi}{\phi(p_\sigma\phi^2 + j\omega p_\varepsilon\phi + j\omega\varepsilon_o\varepsilon_r)}.$$

Defining

$$q = \omega^2 p_\varepsilon^2 + 4j\omega\varepsilon_o\varepsilon_r p_\sigma$$

and then integrating yields

$$\frac{1}{y} = \frac{-1}{2j\omega\varepsilon_o\varepsilon_r\alpha L}\left[-2\gamma + \ln\frac{p_\sigma\phi_o^2 + j\omega p_\varepsilon\phi_o + j\omega\varepsilon_o\varepsilon_r}{p_\sigma\phi_o^2 e^{-2\gamma} + j\omega p_\varepsilon\phi_o e^{-\gamma} + j\omega\varepsilon_o\varepsilon_r}\right.$$

$$\left.\frac{-\omega p_\varepsilon}{q}\ln\frac{(2p_\sigma\phi_o e^{-\gamma} + j\omega p_\varepsilon - jq)(2p_\sigma\phi_o + j\omega p_\varepsilon + jq)}{(2p_\sigma\phi_o e^{-\gamma} + j\omega p_\varepsilon + jq)(2p_\sigma\phi_o + j\omega p_\varepsilon - jq)}\right]. \qquad (36)$$

Again the digital computer was used to compute C/C_o and σ_{eq} for different light intensities. These results are shown in Figure 9 for different dielectric thicknesses and different sensitivities of the permittivity and conductivity to light.

Group B - Uniform Illumination

If $\gamma < 1$, i.e., the dielectric thickness is smaller than an absorption thickness, the models in group A become group B models. The following equation for the normalized admittance is adequate for all of the models in group B:

$$y = \sigma + j\omega\varepsilon = \sigma_o + \sigma_p + j\omega(\varepsilon_o\varepsilon_r + \varepsilon_p). \qquad (37)$$

This is equivalent to assuming that the light intensity is uniform throughout the dielectric material and the material is homogeneous. The problem reduces to determining the variation of conductivity and permittivity with light intensity because there is no variation with position

in group B. The expression is simple enough that it may be evaluated and plotted without the aid of a digital computer. Note the photodielectric effect is absent in group B models unless the microscopic permittivity ε varies with light intensity, i.e., hypothesis two of the introduction does not apply. Figure 10 is a plot of photocapacitance versus equivalent conductivity where $\sigma \propto \phi^{\beta}$ with $\beta = 1/2$, 1 and 2 and $\varepsilon = \varepsilon_o \varepsilon_r + p_\varepsilon \phi$. Increasing the sensitivity of the permittivity to light intensity causes the photocapacitance to become significant at a lower conductivity.

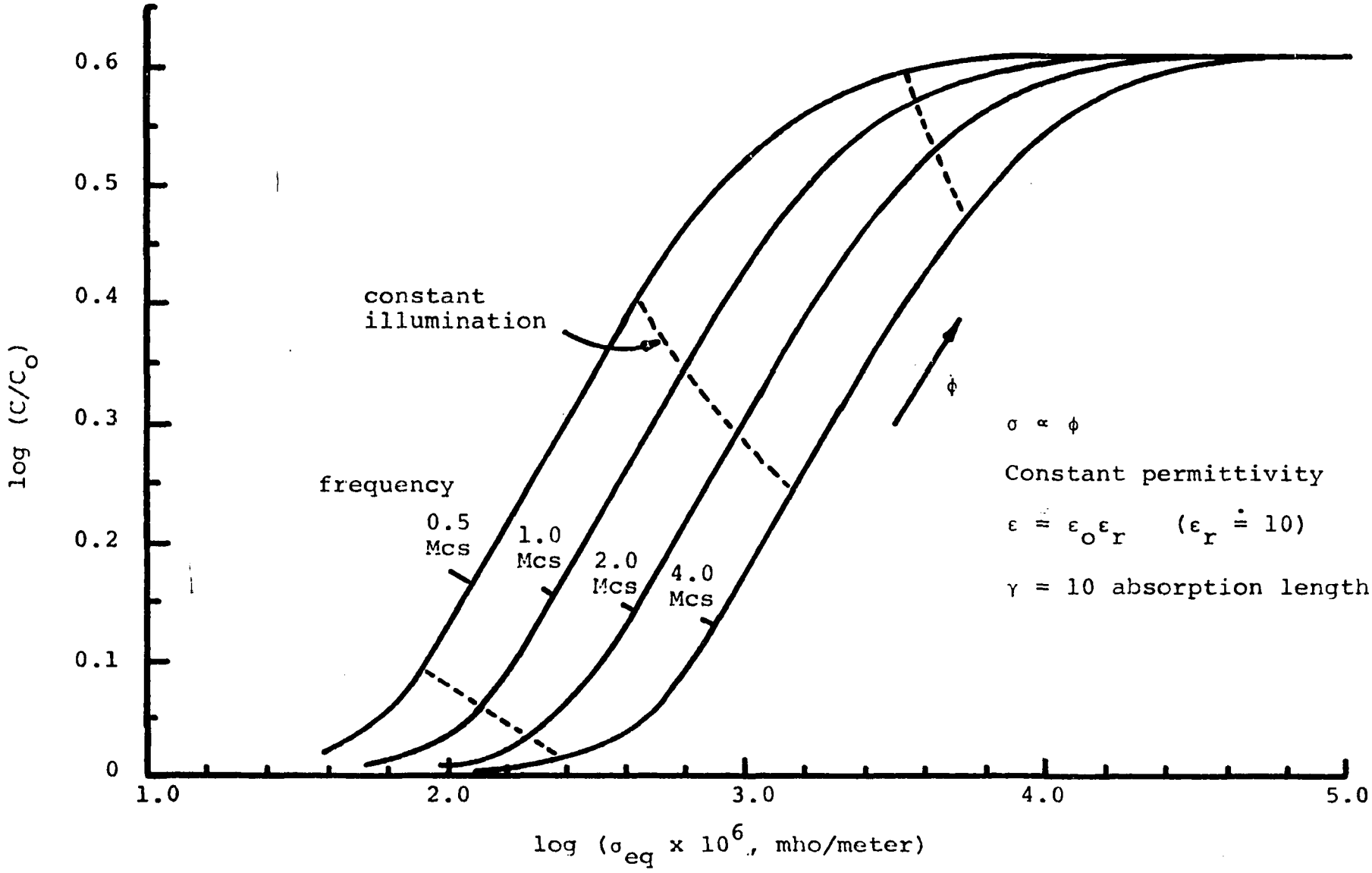

Figure 3. Log normalized capacitance versus log equivalent conductivity for different frequencies. Computer solution, model 1, group A

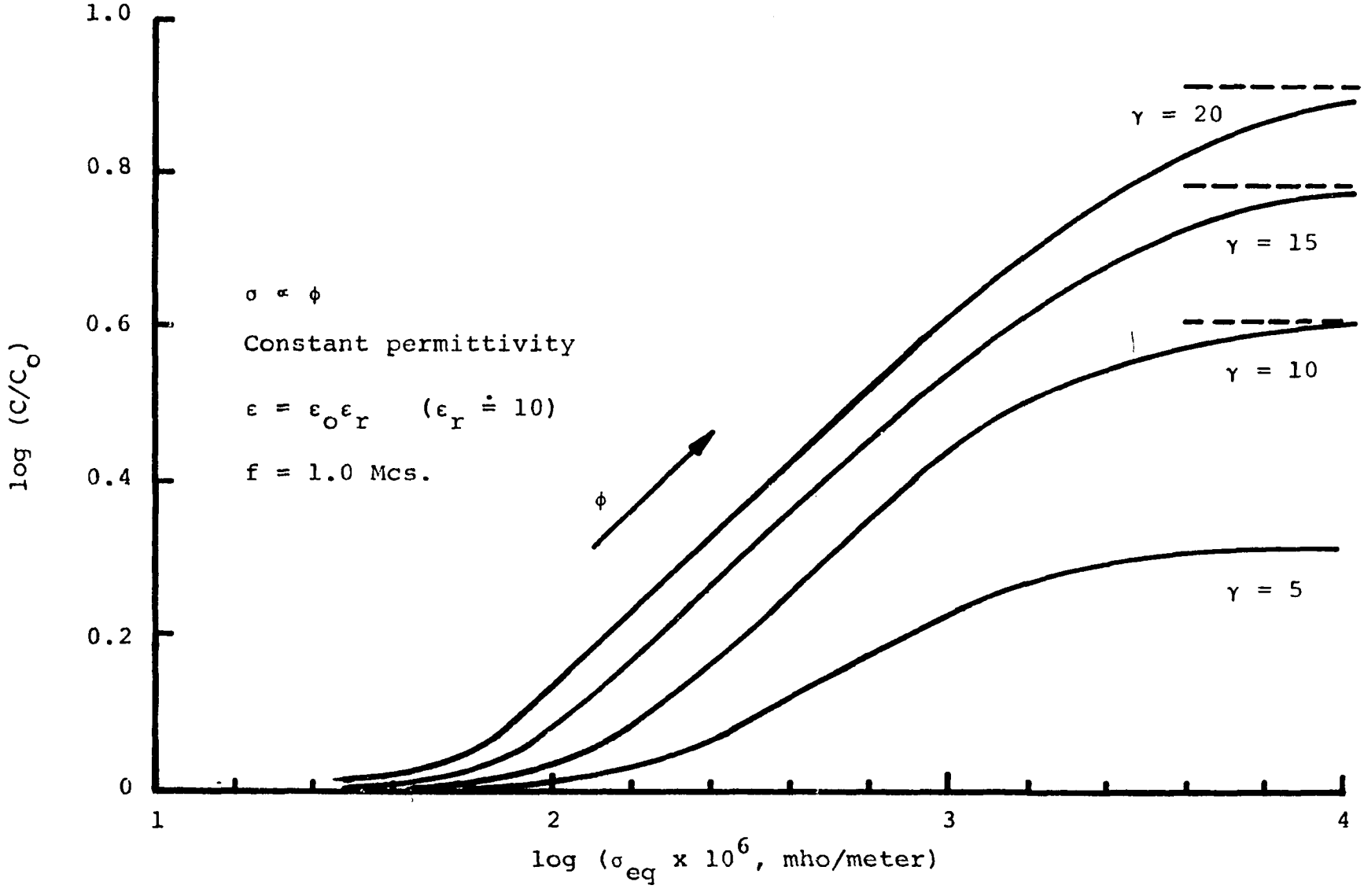

Figure 4. Log capacitance versus log equivalent conductivity showing variation of the photodielectric effect with thickness (in absorption lengths). Model 1 has zero microscopic photodielectric effect. Computer solution, model 1, group A

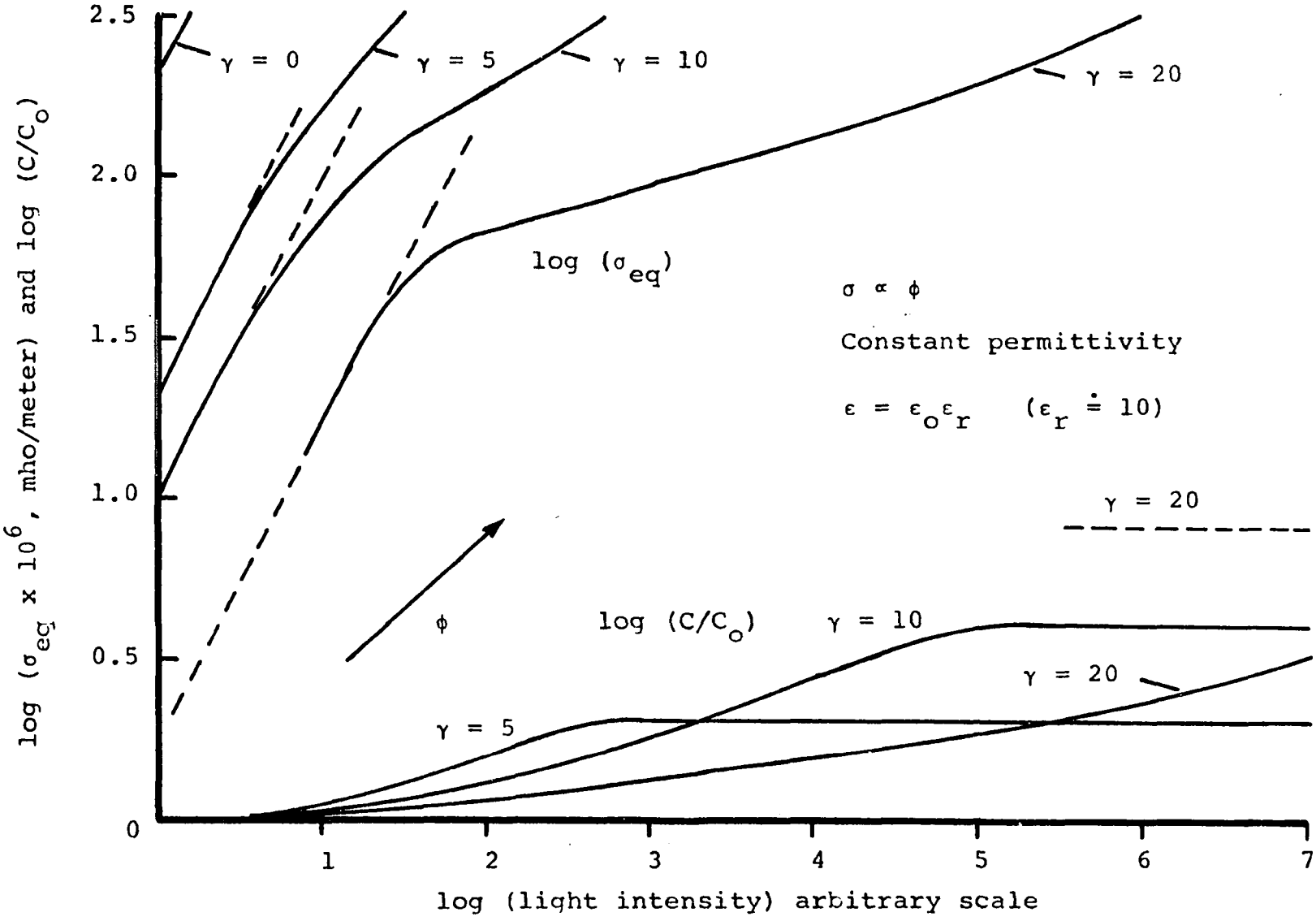

Figure 5. Log capacitance and log conductivity versus log light intensity for different thicknesses (in absorption lengths). Computer solution, model 1, group A

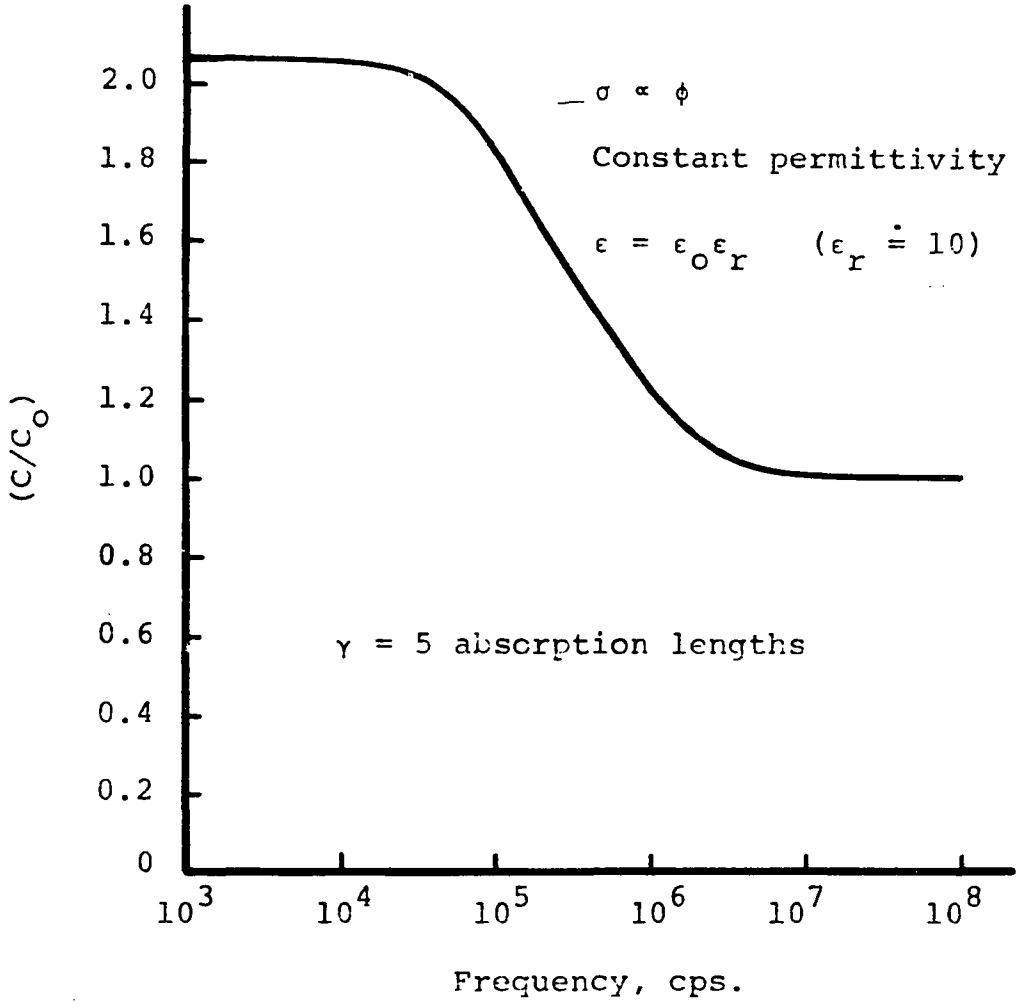

Figure 6. Plot of normalized capacitance C/C_o versus frequency. The permittivity is constant. Model 1, group A

Figure 7. Log normalized capacitance versus log equivalent conductivity for two thicknesses, showing the effect of microscopic photodielectric effect. Computer solution, model 2 and model 1, group A

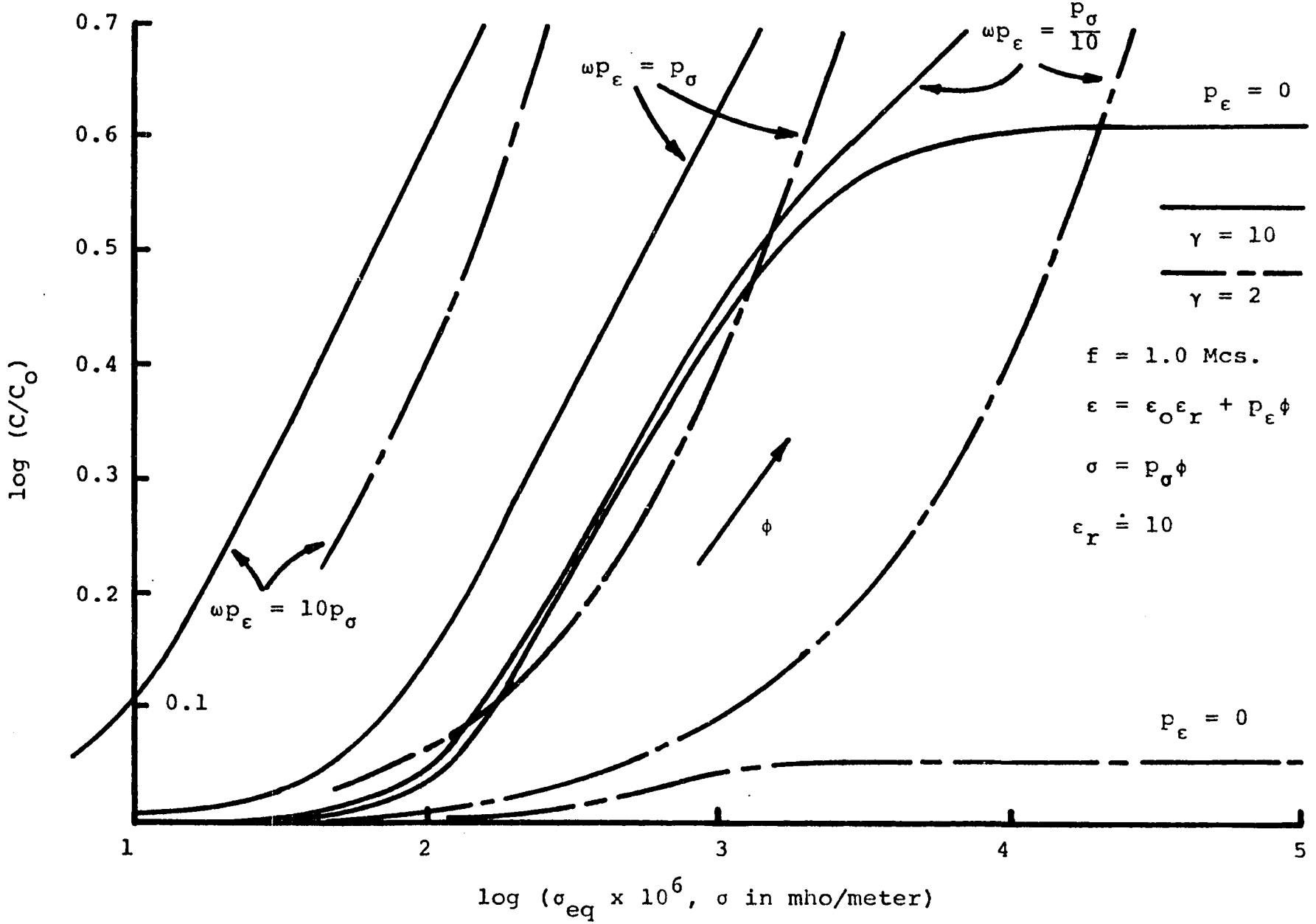
0.7
0.6
0.5
0.4
0.3
0.2
0.1
log (C/C$_o$)
1
2
3
4
5
log (σ_{eq} x 10^6, σ in mho/meter)
$\omega p_\varepsilon = \frac{p_\sigma}{10}$
$\omega p_\varepsilon = p_\sigma$
$\omega p_\varepsilon = 10 p_\sigma$
$p_\varepsilon = 0$
$p_\varepsilon = 0$
$\gamma = 10$
$\gamma = 2$
f = 1.0 Mcs.
$\varepsilon = \varepsilon_o \varepsilon_r + p_\varepsilon \phi$
$\sigma = p_\sigma \phi$
$\varepsilon_r \doteq 10$
ϕ

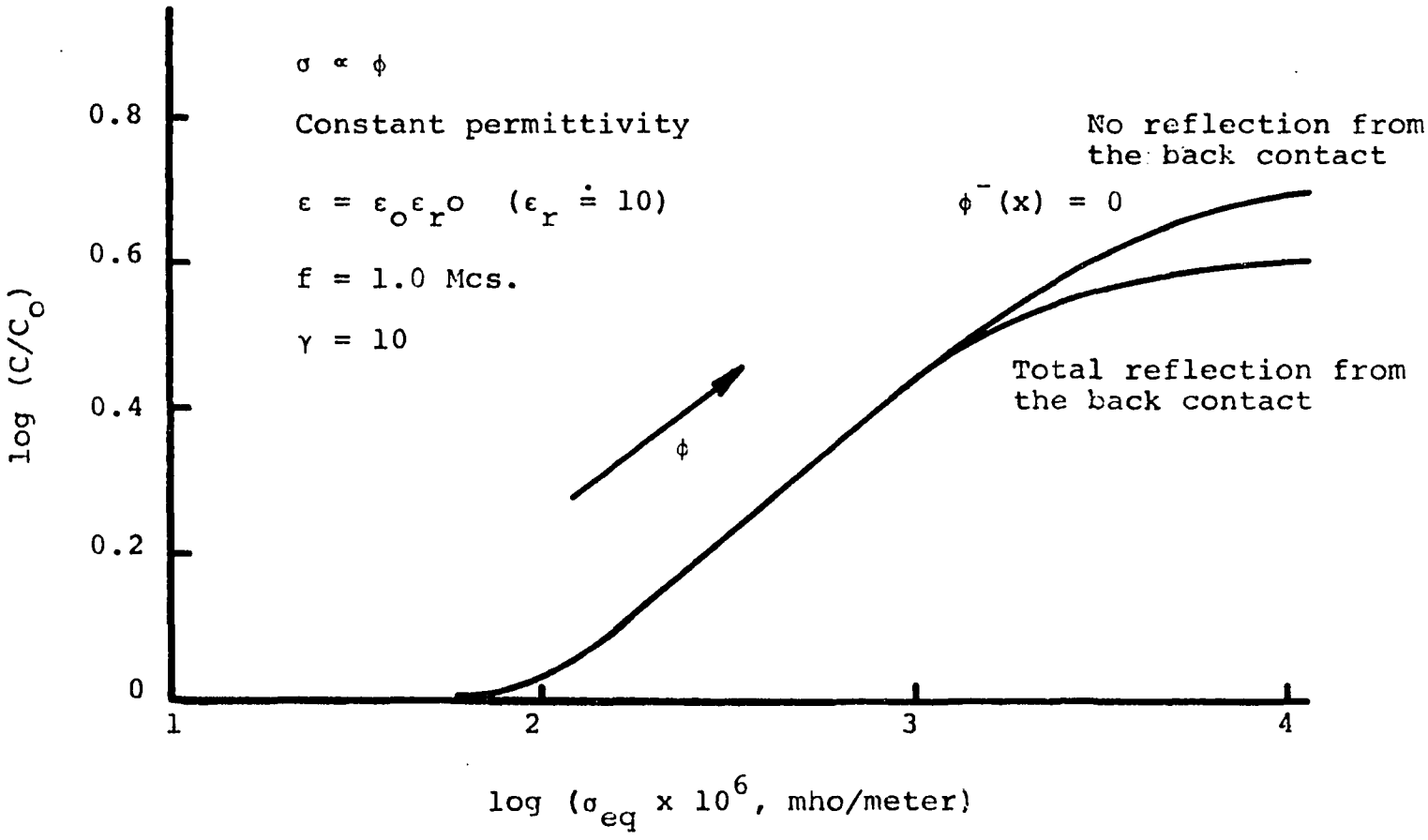

Figure 8. Log normalized capacitance versus log equivalent conductivity showing the computed difference between total reflection and zero reflection from the back contact. Computer solution, models 1 and 3, group A.

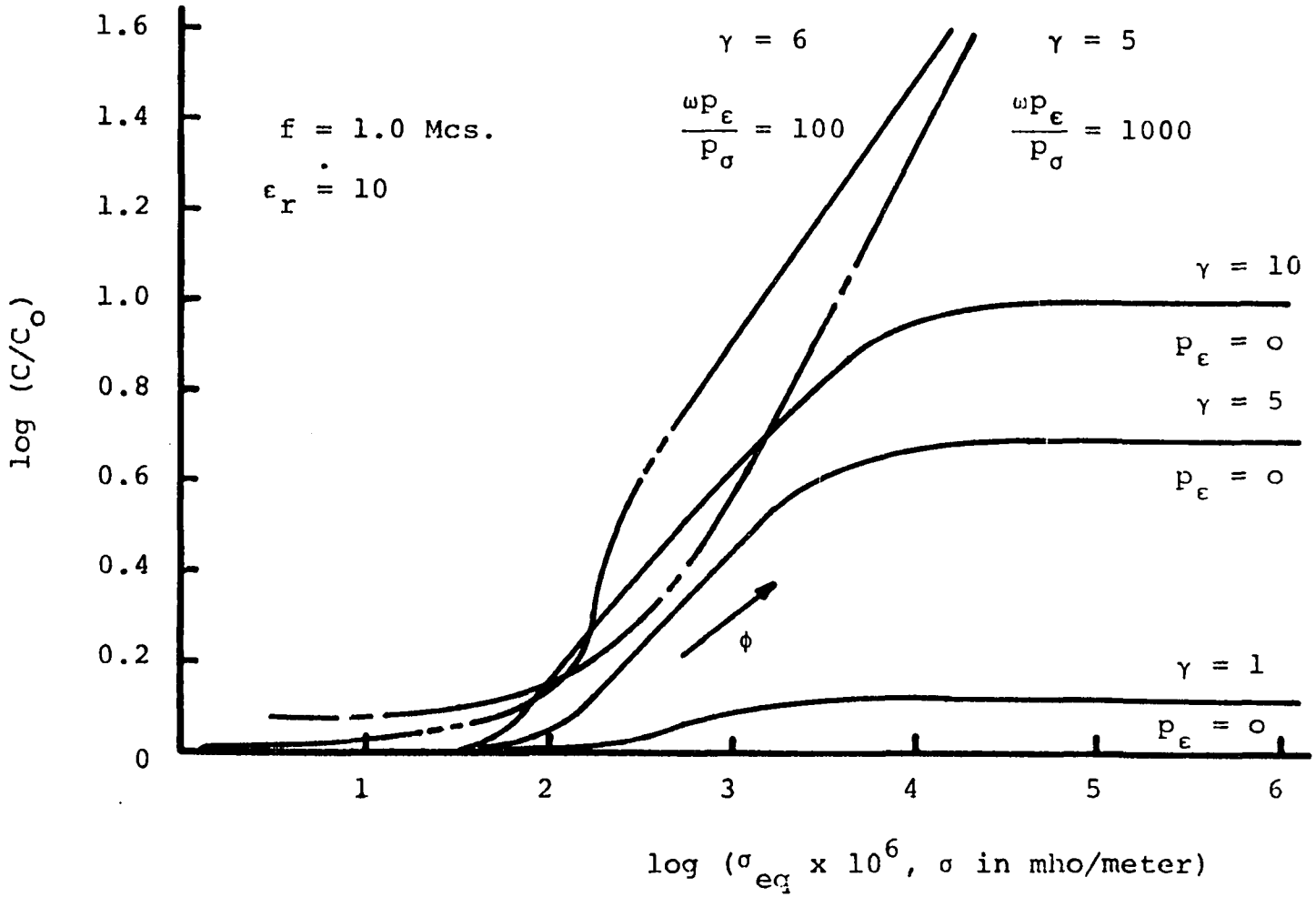

Figure 9. Log normalized capacitance versus log equivalent conductivity. $\sigma = p_\sigma \phi^2$ and $\epsilon = \epsilon_o \epsilon_r + p_\epsilon \phi$. Computer solution, model 4, group A. (Supralinear conductivity)

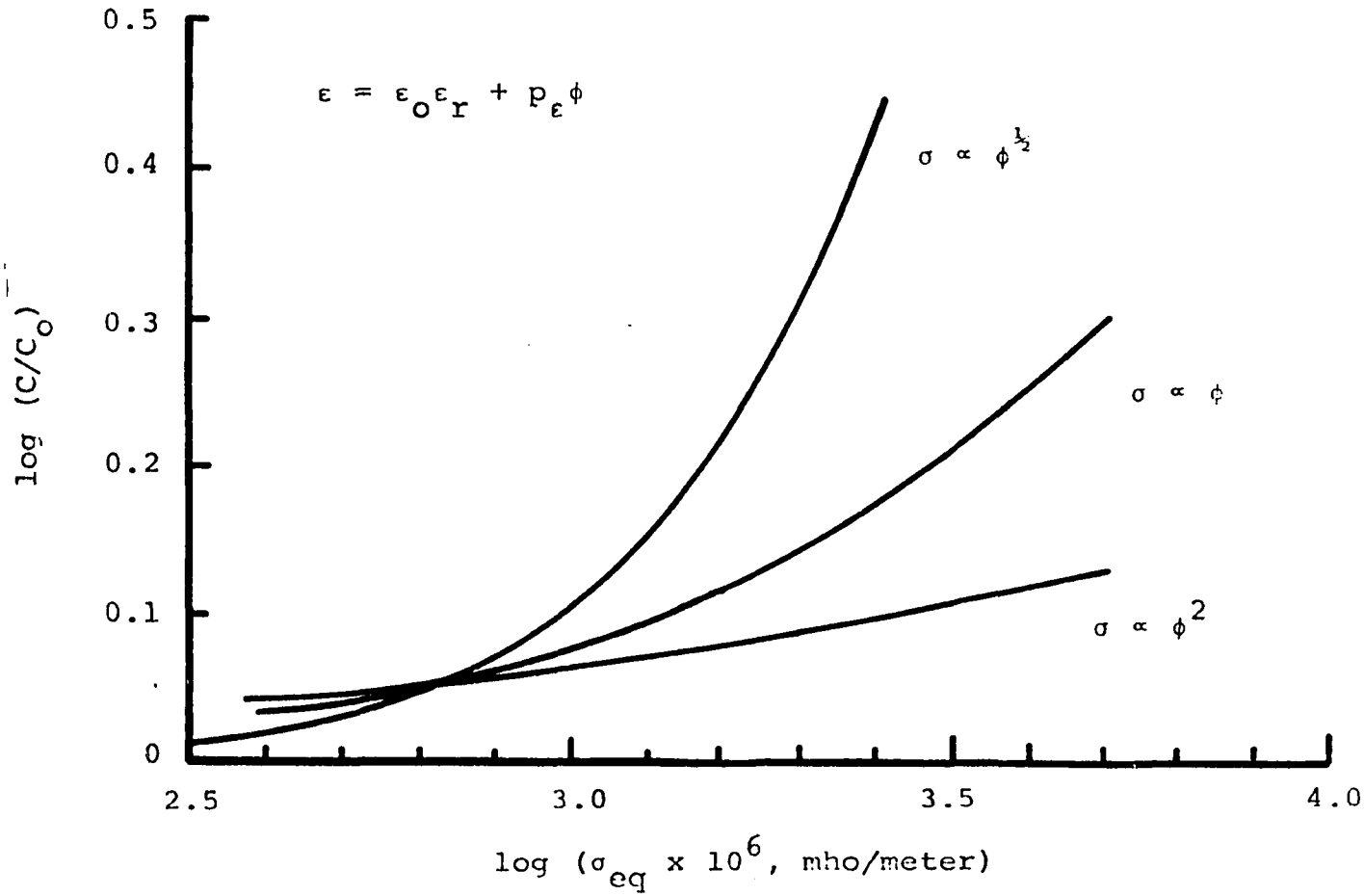

Figure 10. Log normalized capacitance versus log equivalent conductivity. Computed results for models 1, 2 and 3, group B

EXPERIMENTAL METHODS AND RESULTS

This section describes the preparation of a photocapacitor having a CdS single-crystal dielectric and the techniques used to measure its admittance over a range of frequencies and light intensities. The optical transmission properties and the variation of conductivity with light intensity are also measured for the CdS dielectric.

CdS Photocapacitor

The experimental results reported in this section were all obtained from a plate cut from a 92 gram single-crystal of cadmium sulfide (CdS) purchased from the Eagle-Picher Company. CdS was used because it is very photosensitive and large single-crystals are available. Typical material parameters of CdS are listed in Table 3.

Table 3. Properties of cadmium sulfide

Crystal symmetry	hexagonal (6mm)
Band gap energy (4)	2.4 ev.
Absorption edge (4)	500 mμ
Specific weight (1)	4.82
Dielectric constant (1)	10.3 (dark)
Preparation	grown from vapor phase
Soluble	HNO_3
Melting point	1500°C (50 atm. argon)

The crystal was oriented by conventional x-ray diffraction techniques, and a plate was cut from it with the face parallel to the hexagonal axis. A number of problems arise in attempting to apply conventional strain-free cutting techniques to CdS crystals; its conductivity is too low

for a spark cutter and when an acid saw is used, a sulfur residue produced by the reaction of CdS and HNO_3 interferes with the cutting and leaves a very rough surface. Both of these techniques were tried, but ultimately it was necessary to resort to a diamond saw. The cut was made with two four-inch diameter blades separated by a 54 mil shim. Attempts to make cuts perpendicular to the c-axis failed because the crystal tends to cleve along that axis and the vibration of the saw was sufficient to fracture the crystal.

The edge of the plate was etched in concentrated HNO_3 to remove the stress concentration points. After lapping to obtain flat surfaces, the thickness of the plate was measured with a micrometer. Next, it was polished manually with 400, 600 and 1200 mesh silicon carbide and then with 1.0, 0.3 and 0.05 micron alumina (Al_2O_3) in that order. The polishing was done on plate glass with a distilled water vehicle. The polished crystal was first cleaned in acetone, then trichloroethylene and finally it was suspended in an alcohol vapor degreaser for several minutes. After cleaning, the CdS plate was placed on a mask in a vacuum chamber for deposition of the electrical contacts.

Contacts

Considerable information has been published about electrical contacts to cadmium sulfide (2, 3, 10, 25, 27, 29). Indium and gallium are usually used if ohmic contacts are required; while gold, which may be used for transparent contacts, forms a rectifying contact. Sihvonen and Boyd (27) have described a technique to obtain transparent ohmic contacts to CdS by

diffusing indium into the surface of the material. This technique is reported to produce surface resistances as low as 12 ohms/square with changes of less than one percent in the transmittance properties of CdS from the band edge to 20,000 A. However, the contacts for this investigation were deposited in a vacuum before the preceding technique was known. Aluminum was used for the semitransparent contact after several attempts with indium and gallium. Indium and gallium were both opaque when enough material was deposited to form a low resistance contact. An indium contact was deposited on the side of the CdS plate that did not pass light. The surface resistance was monitored during deposition of the aluminum on the CdS plate by placing a microscope slide with contacts next to the CdS plate. The measured surface resistance was in agreement with calculations based on the following assumptions: 1) the volume of the aluminum was known, 2) the material would be deposited uniformly over a hemisphere and 3) all of the aluminum would be deposited without reacting or alloying with the tungsten filament (12, 23). The electrical connections from the contacts to the external circuit was made with aluminum foil and silver paint. The resulting photosensitive capacitor may be represented by Figure 2 even though the edges are irregular. All of the experimental data was taken on a crystal 26 mils (0.66 mm) thick with an irregular contact area of 3.4 cm^2.

Optical Measurements

Optical transmission measurements were made for the CdS plate and the aluminum contact separately. The sample was illuminated with an

incandescent light source and the incident and transmitted light intensity was measured at several wavelengths with a spectrophotometer. The output of the RCA 5819 photomultiplier tube in the spectrophotometer was monitored on an oscilloscope. Figure 12 shows the optical transmission as a function of wavelength for the aluminum contact on a glass substrate, for the glass substrate alone, and for the 26 mil CdS plate without the contacts. The data show the aluminum contact acts as an optical filter with a bandwidth of approximately 55 mμ centered at 350 mμ, a strong absorption region for CdS. The aluminum contact has a surface resistance of about 10 ohms per square which corresponds to a thickness of 300 mμ if the film is homogeneous. The glass substrate passes between 80 and 90 percent of the light in the region of interest and may be neglected. Figure 12 shows an absorption edge of approximately 500 mμ in CdS. This agrees with published data (3, 4), and corresponds to a gap energy of approximately 2.4 ev.

A relative measurement of the light intensity output of the incandescent source in the absorption region of CdS was determined as a function of applied voltage. A number 38 A blue-pass Wratten filter was placed between the source and a light meter to obtain the calibration curve plotted in Figure 16. This information was required to experimentally determine the variation of conductivity with light intensity.

Electrical Measurements

The parallel resistance and capacitance of the CdS photocapacitor were measured with a modified Boonton RX meter (type 250-A). The instrument is completely self-contained and consists of a Schering bridge,

oscillator, power supply and null detecting circuit. When the bridge is balanced, the parallel resistance and parallel capacitance of an unknown can be read directly from two calibrated dials. At balance, 100 mv is applied to the unknown. The equations for balance of the Schering bridge circuit shown in Figure 11 are

$$\frac{R_2}{C_p} = \frac{R_3}{C_1} = \frac{R_p}{C_2}, \tag{38}$$

where $C_p = C_4 + C_x$ and $1/R_p = 1/R_4 + 1/R_x$. C_2 and C_4 are variable precision air capacitors used to balance the bridge when an unknown R_x and C_x are connected to terminals C-D. Solving for the unknowns,

$$C_x = R_2(C_1/R_3) - C_4 \tag{39}$$

and

$$R_x = \frac{R_4 R_3 C_2}{R_4 C_1 - R_3 C_2}. \tag{40}$$

In Equation 39, R_2, C_1 and R_3 are constant and known; therefore, C_4 is a linear measure of C_x. In Equation 40, R_4, R_3 and C_1 are constant and known, and the remaining parameter C_2 may be calibrated to read R_x.

Originally the RX meter was designed to measure both capacitive and inductive unknowns, and C_4 read from -100 to +20 pf. For this research, the bridge was modified to measure C_x from 0 to 120 pf by changing R_2 so that the bridge was balanced when

$$C_4' = C_4 - 100 \text{ pf} = C_4 - \Delta C$$

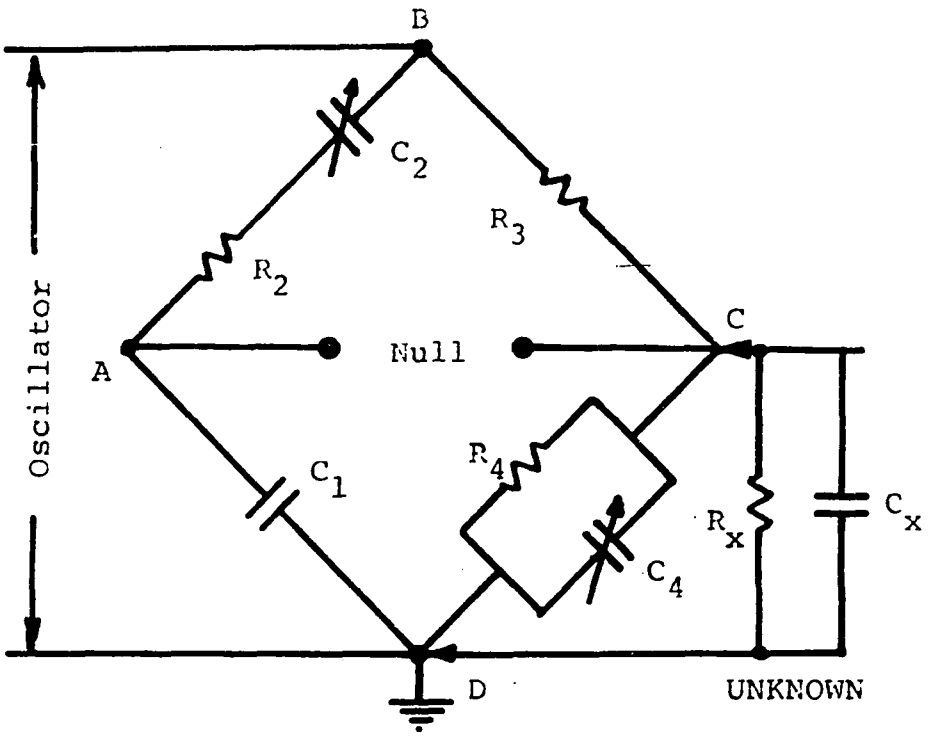

$$C_p = C_4 + C_x$$

$$\frac{1}{R_p} = \frac{1}{R_4} + \frac{1}{R_x}$$

Balance equations

$$Z_{AB}Z_{CD} = Z_{AD}Z_{CB}$$

$$\frac{R_3}{C_1} = \frac{R_2}{C_p} = \frac{R_p}{C_2}$$

Figure 11. Schering bride circuit

R_2 does not appear in Equation 40 and therefore does not change the calibration of the resistive measurement. The new value for R_2 is

$$R_2' = R_2 - R_3(\Delta C/C_1). \tag{41}$$

Capacitance readings were made on the modified bridge by adding a ΔC of 100 to the indicated readings.

Two #12 wires, 8 inches long, were used to connect the CdS capacitor to the terminals of the RX meter. The instrument was nulled before each reading with the wires connected to the instrument but not to the CdS capacitor. Even though the wires were separated, their distributed impedance became significant at a few megacycles when the light intensity was high and the impedance of the CdS capacitor was small. An equivalent circuit for the wires was determined and the data was corrected when necessary.

The measurements made with the Boonton RX meter are presented in Figures 13, 14 and 17 as normalized parallel capacitance and equivalent conductivity.

$$\text{Normalized parallel capacitance} = C_x/C_o = C/C_o. \tag{42}$$

$$\text{Equivalent conductivity} = \sigma_{eq} = L/(AR_x). \tag{43}$$

Several readings of capacitance and equivalent conductivity were made at -5° C and a few readings were taken at temperatures between -5° and room temperature. The lower temperatures were obtained by mounting the CdS capacitor in an insulated box 4 by 4 by 7 inches containing dry ice. The

box was mounted directly over the input terminals of the RX meter to minithe lead length and the CdS dielectric was not illuminated. These measurements indicated that temperature control device that had been designed would not be needed, consequently the data presented were obtained at room temperature.

Figure 13 is a log-log plot of the normalized capacitance versus the equivalent conductivity. Curves are shown for four different frequencies. Incident light intensity (not measured) increases with increasing conductivity.

Figure 14 is a plot of the transient of parallel capacitance and equivalent conductivity for a step change in light intensity from strong illumination to zero illumination. The transient was slow enough that the bridge could be balanced manually every 20 to 30 seconds to obtain the data.

Figure 17 is a plot of the variation of equivalent conductivity and parallel capacitance with light intensity. The optical measurements required for this curve were discussed earlier in this section. Figure 17 indicates that the conductivity varies as the square root of light intensity for the CdS photocapacitor used in this investigation. The data for the variation of capacitance with light intensity are not sufficient to determine what slope the curve is approaching, however, the dotted line on the graph would correspond to a unit slope or linear variation of capacitance with light intensity at high light intensities.

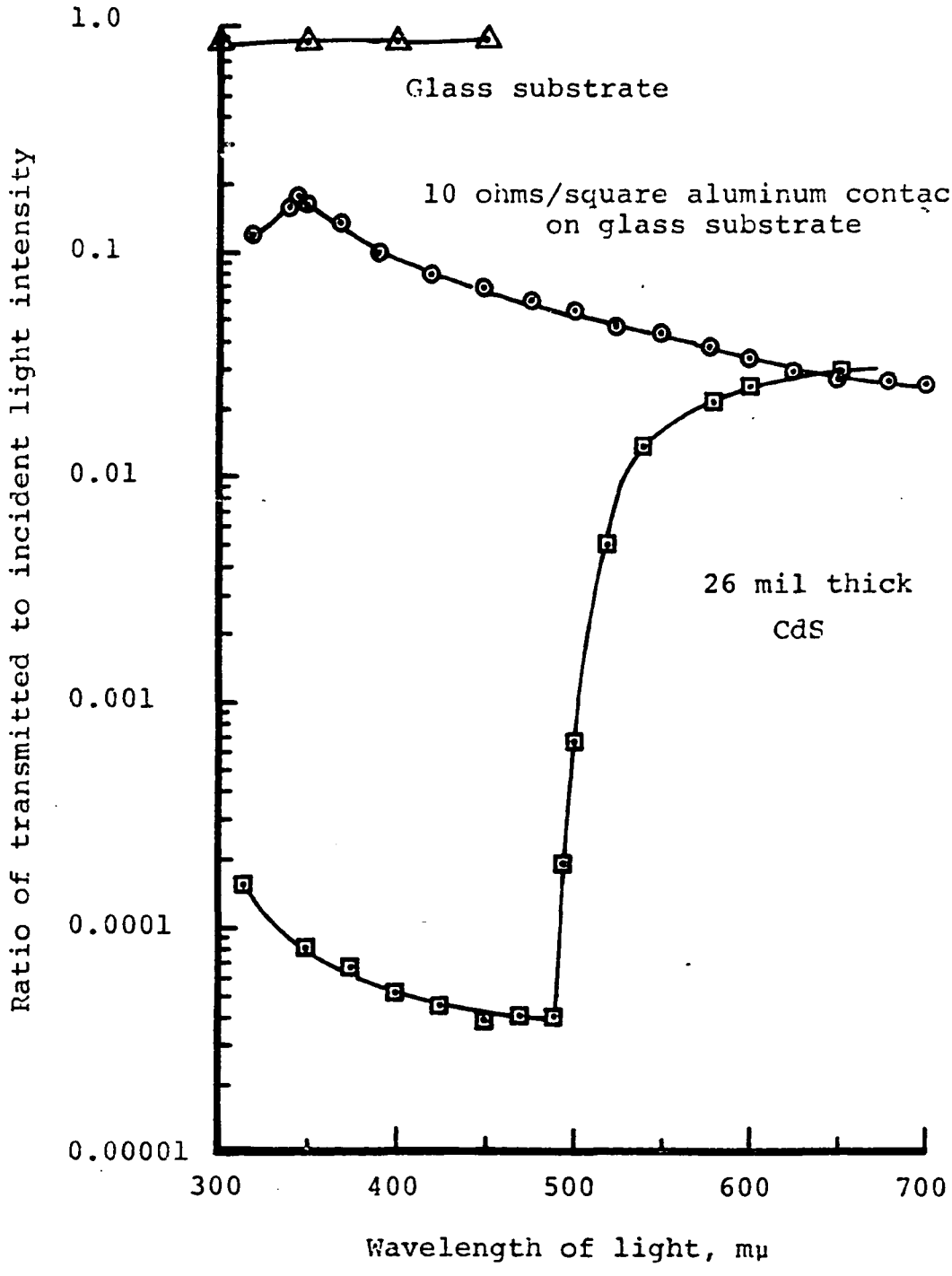

Figure 12. Optical transmission properties of CdS and semitransparent aluminum contact

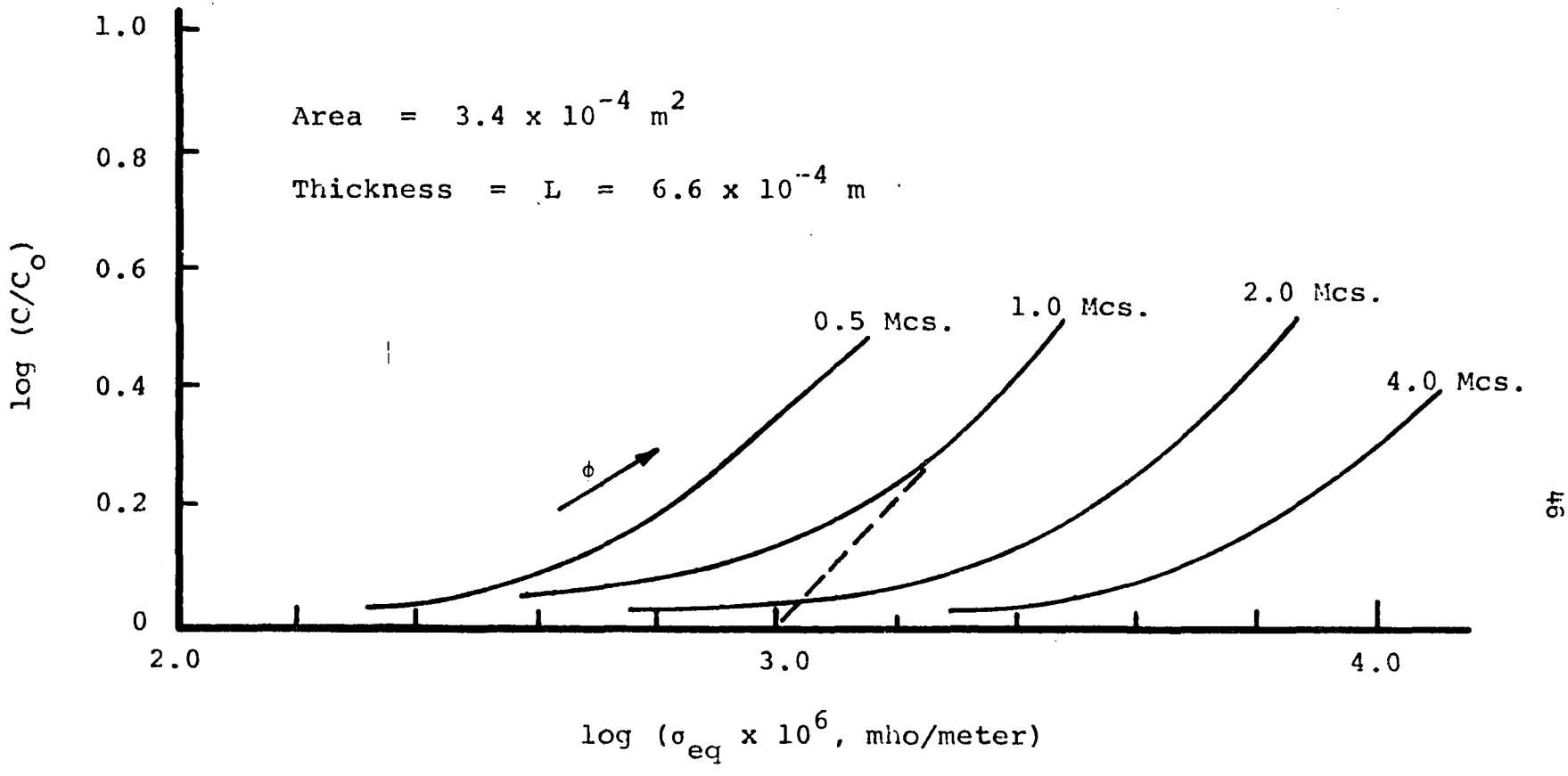

Figure 13. Experimental data, CdS single crystal photocapacitor. Log normalized capacitance versus log equivalent conductivity for 4 frequencies

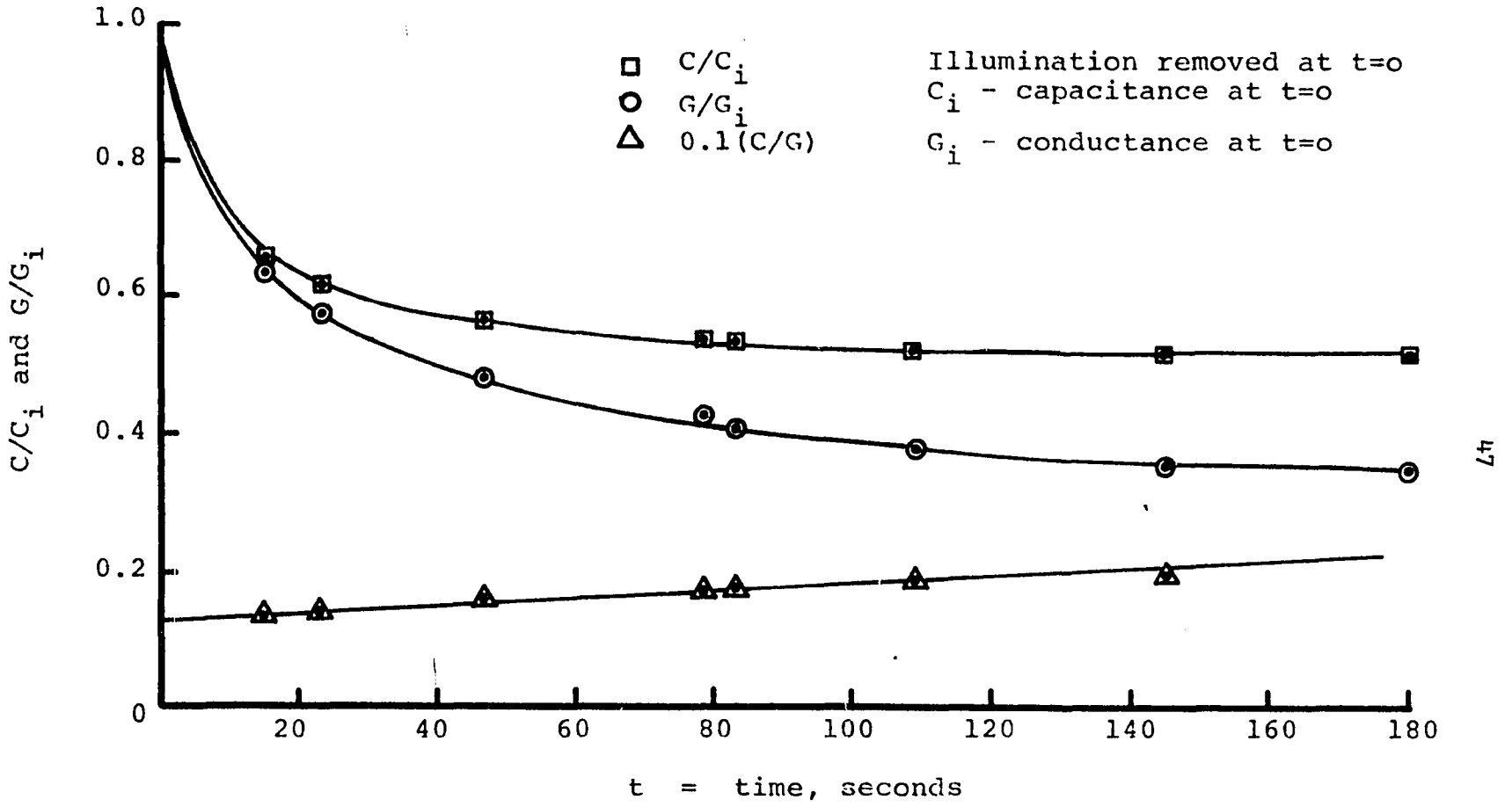

Figure 14. Experimental transient data for CdS photocapacitor. Steady-state a.c. parameters and a step change in light intensity. The "time constant" RC = C/G is also plotted

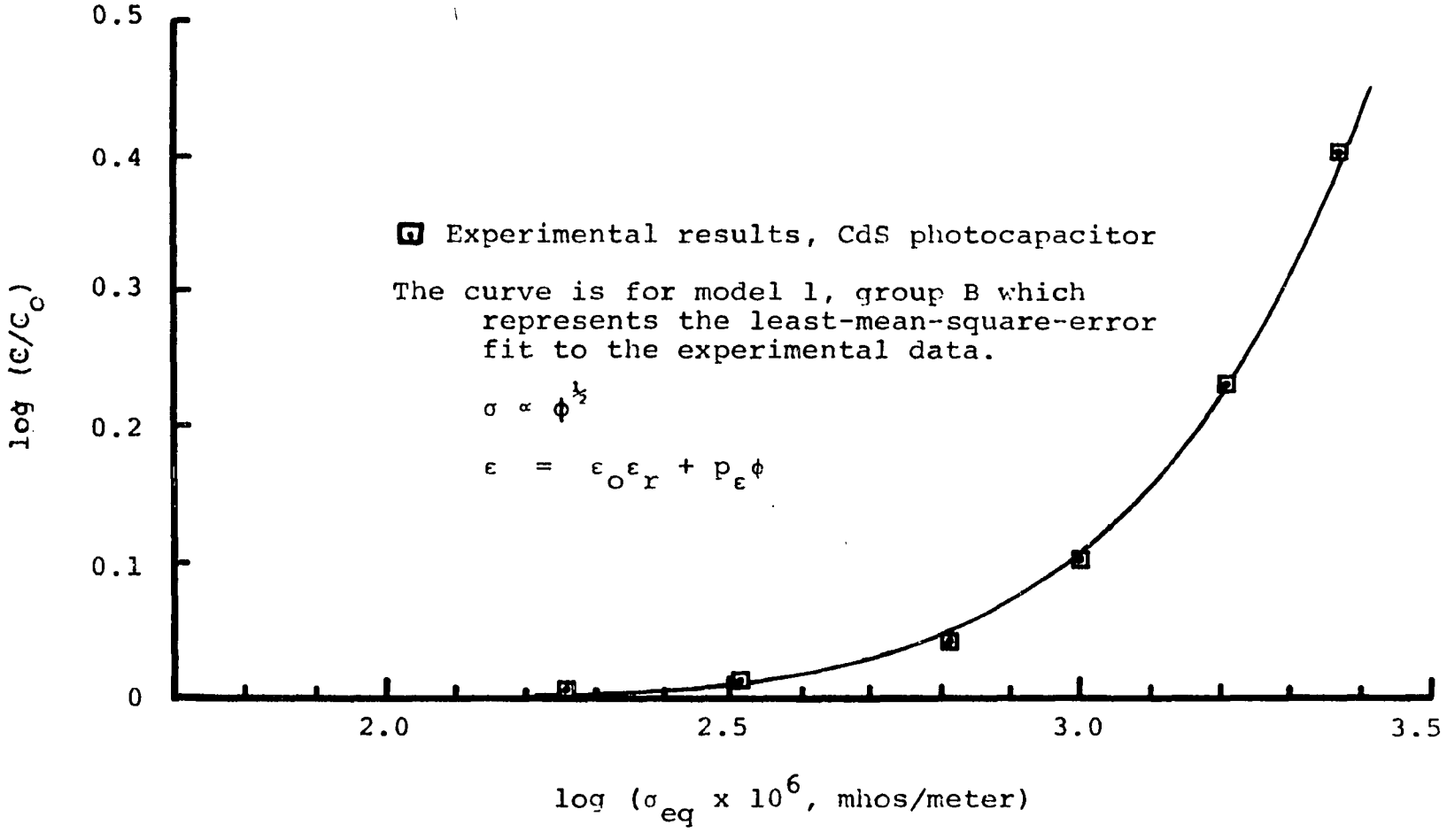

Figure 15. Log normalized capacitance versus log equivalent conductivity showing experimental results for the CdS capacitor and the least-mean-square-error model

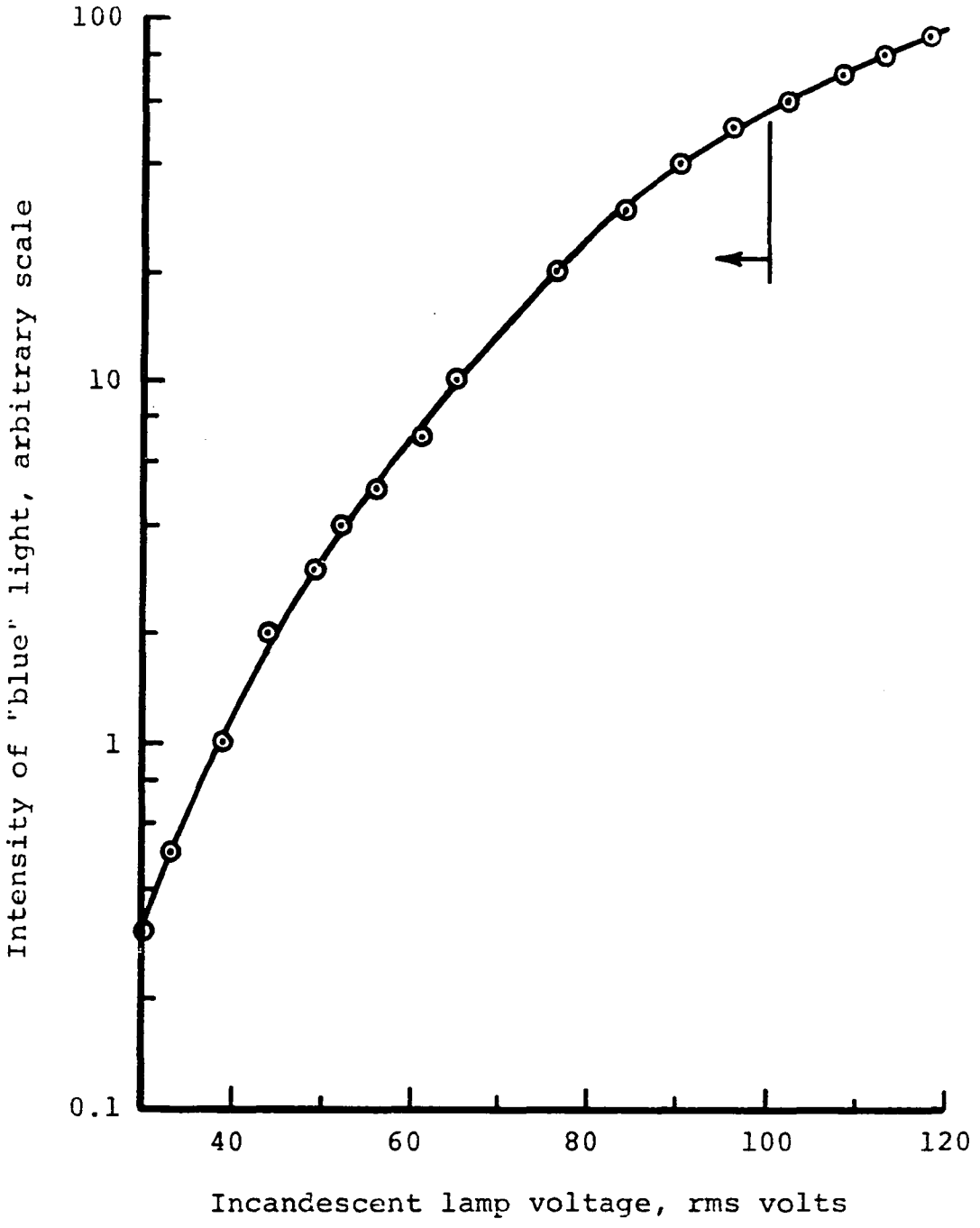

Figure 16. Calibration curve for a typical 50w, frosted, incandescent lamp

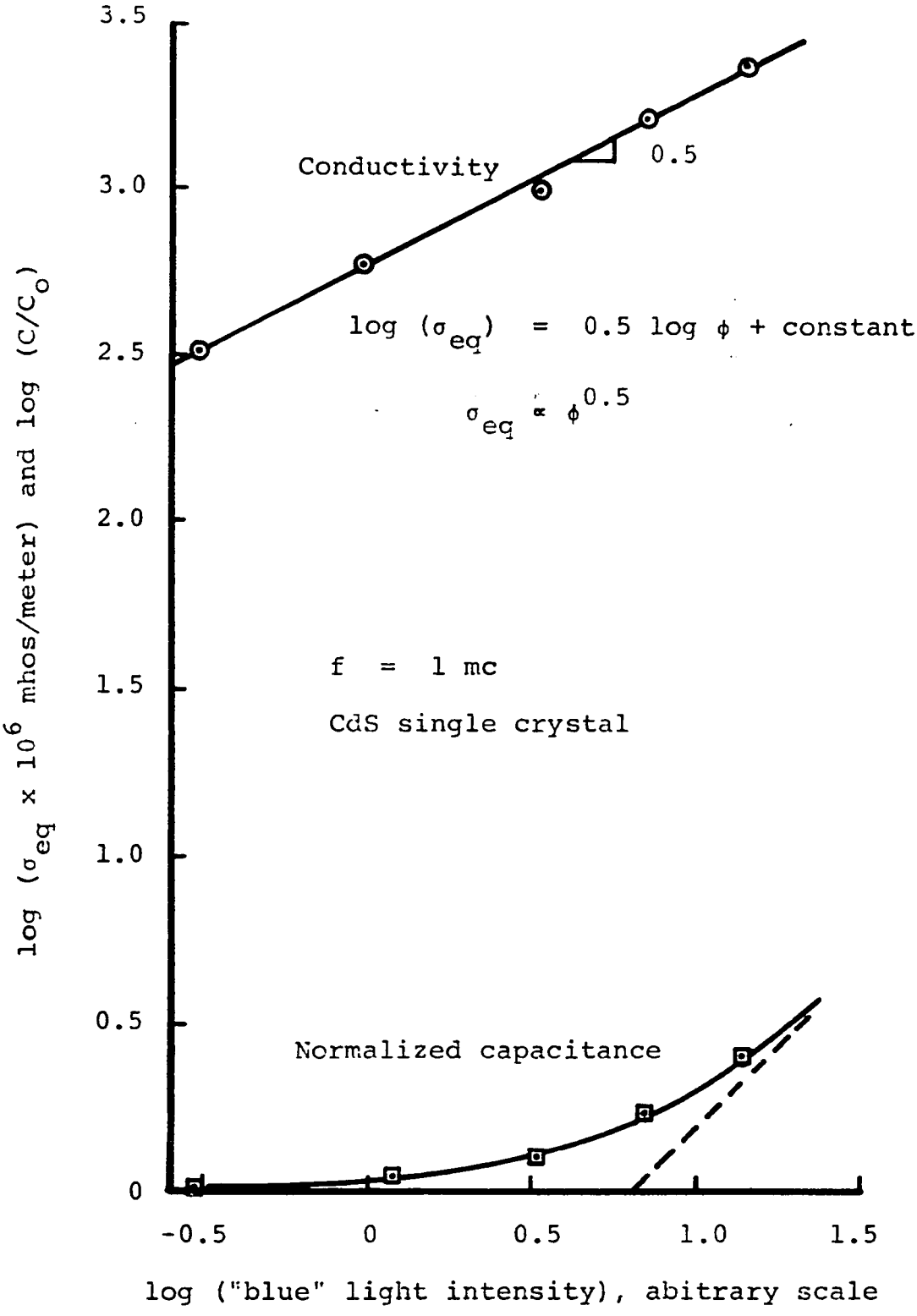

Figure 17. Plot of conductivity and capacitance variation with light intensity. Dotted line has a slope of unity. Experimental CdS photocapacitor data

CONCLUSION

In this section, the photodielectric hypotheses and the significance of the data obtained from the mathematical models are discussed. A model representing the experimental photocapacitor data is presented and the parameters giving the least-mean-square-error fit to the data are derived.

The mathematical models for the photodielectric effect demonstrate two of the three hypotheses discussed in the introduction. The data obtained from the models indicate that both hypotheses are correct. For a given photocapacitor, either hypothesis could be correct and, in some cases, both mechanisms are required. This conclusion is in agreement with Bube (3) who states that each of the three hypotheses has its own region of application and in some cases all three processes are involved simultaneously. This explains the apparently conflicting conclusions of published results. Each device must be examined separately to determine which mechanisms contribute significantly to the increase in capacitance with radiation.

Results - Group A Models

The models in group A are all based on variation of light intensity with position in the dielectric. Figures 3 through 9 show the results of the digital computer solution of those models. The dark dielectric constant of CdS was used in the computer solutions so that the models could be compared with the experimental results. Figures 3 through 6 demonstrate hypothesis 2 of the introduction. The variation of light intensity with position causes a corresponding variation of conductivity with

position. The region nearest the illuminated surface has a relatively high conductivity, and the conductivity decreases monotonically with distance from the illuminated surface. The result is an effective reduction in the thickness of the insulating region. This causes an increase in the terminal capacitance even though it is assumed that the permittivity does not change. Figures 3 through 6 contain the results of the solution of model 1, group A.

Figure 3 (group A - model 1) is a log-log plot of the normalized parallel capacitance versus the equivalent conductivity of a dielectric 10 absorption lengths thick. Increasing illumination causes the loci of the curves to move from left to right. Curves for five different frequencies are plotted. This type of plot is one way of characterizing photoeffects in terms of electrical quantities and does not require optical measurements. Comparing Figure 3 and the experimental results in Figure 13 shows general agreement in the curves before saturation of the photocapacitance in the model. A closer examination of the data for the CdS device reveals that the conductivity at which the photocapacitance becomes significant is at least 10 times greater than the model. This is true of all the models in group A. The rate at which the capacitance changes with respect to the conductivity also indicates that the group A models do not represent the experimental work of this dissertation.

Figure 4 (group A - model 1) is also a log-log plot of capacitance similar to Figure 3, but the frequency is constant and the dielectric thickness varies. This curve shows that the photodielectric effect is greater for thicker dielectrics. The fit with experimental data is not improved by changing the thickness of the material.

Figure 5 (group A - model 1) is a log-log plot of equivalent conductivity and parallel capacitance versus light intensity. This graph indicates a change in capacitance without a permittivity change as did the previous two graphs but, in addition to this, it predicts that the equivalent conductivity tends to saturate at higher light intensities even though the conductivity is varying linearly. The deviation from linearity becomes more pronounced for thicker dielectrics. The lack of correlation between the group A models and the experimental data is again demonstrated by comparing Figures 5 and 17 which are plots of the same variables. Figures 3, 4 and 5 demonstrate the importance of the second hypothesis with increasing dielectric thickness.

Figure 6 is a plot of the parallel capacitance computed from model 1 (group A) as a function of frequency. As the frequency increases, the capacitance decreases to a lower value. An obvious conclusion from the curve would be that the material contains polarizable centers with finite relaxation times. This is a false conclusion for this model because one of the model specifications is that the permittivity does not change under any circumstance. The change in capacitance with frequency occurs because the material near the illuminated contact is resistive and the material near the other contact acts as a dielectric. Consequently the photocapacitor is roughly equivalent to a resistor and a capacitor in series. At low frequencies, the electric field would be mostly across the nonconducting or dielectric region of the photocapacitor. At higher frequencies, the field would tend to be distributed across the material and, because the permittivity does not change, this would cause the parallel capaci-

tance at the terminals to decrease. Once again the importance of the variation of light intensity with position has been demonstrated.

A log-log plot of normalized parallel capacitance as a function of equivalent conductivity is plotted in Figure 7 to show the effect of varying the permittivity linearly with light intensity (group A - model 2). This computer solution for different dielectric thicknesses indicates that the addition of the light sensitive permittivity specification causes an even greater increase in the capacitance than was observed in model 1. Results computed from model 1 are also plotted in Figure 7 for comparison.

Figure 8 is a digital computer solution for models 1 and 3 (group A) showing the difference between specifying zero reflection and total reflection from the back contact. The difference is significant at high light intensities only.

A computer solution of the capacitance and equivalent conductivity for model 4, group A, is plotted in Figure 9. The conductivity varies as the square of light intensity; however, other powers greater than one would also be acceptable. Such a variation of conductivity is called supralinear and is discussed in the introduction. The results are plotted for three different dielectric thicknesses with constant permittivity specified and for two thicknesses with linear variation of the permittivity with respect to light intensity. A digital computer program was written for model 4 to solve for the parameters that result in the least-mean-square-error fit with experimental data. The program determined the optimum values for dielectric constant, thickness and the sensitivity of permittivity and conductivity to light.

The importance of examining the contribution of the variation of light intensity with position to both photoconductivity and the photodielectric effect has been demonstrated by the digital computer solutions of the group A models. The variation of light intensity with position together with even linear variation of conductivity with light intensity and no change in the permittivity offers an explanation for 1) the photodielectric effect, 2) saturation of the photocapacitance, 3) nonlinear variation of equivalent conductivity with light and 4) for an apparent dielectric relaxation phenomenon.

Results - Group B Models

As previously discussed, if the dielectric material in a photocapacitor is thinner than an absorption length, the normalized a.c. admittance y is related to the conductivity and permittivity by the equation

$$y = \sigma + j\omega\varepsilon.$$

The most important result of this restriction is that any photodielectric effect for homogeneous materials in the group B models must be due to an actual change of the permittivity. That is, hypothesis 2 of the introduction will not apply because the light intensity is uniform throughout the material.

Figure 10 (group B - models 1, 2 and 3) is a log-log plot of the parallel capacitance versus the equivalent conductivity for three different variations of conductivity with light intensity. In each model the

permittivity varies linearly with light intensity. The phase angle of the admittance associated with the region where the capacitance change becomes significant is a measure of the sensitivity of the permittivity to light. In other words, if the permittivity is relatively insensitive to light, the conductivity will be quite high before the permittivity increase becomes significant and the phase angle will be small.

Model to Fit Experimental Data

The experimental data for the photocapacitor presented in this dissertation may best be represented by a model from group B with

$$\sigma = p_\sigma \phi^{1/2} \tag{44}$$

and $$\varepsilon = \varepsilon_o \varepsilon_r + p_\varepsilon \phi^1. \tag{45}$$

Three steps are required to determine the above model.

The first step in matching a mathematical model to the CdS photocapacitor data is to determine whether the dielectric should be classified as "thick" (group A) or "thin" (group B). This may be done by observing the equivalent conductivity at which the increase in capacitance becomes significant. If the knee of the capacitance versus equivalent conductivity curve occurs above a certain critical conductivity, the device may be represented by a group B model only. If the knee is below the critical value, additional information is required to determine whether the capacitance increase is due to hypothesis 1 or hypothesis 2 (group A) or both. It is important to note that the "dark" permittivity and the "dark"

conductivity must be known before the curves for the models can be plotted; therefore, if a material other than CdS is used, other curves would be required. For CdS, if the equivalent conductivity at the knee of the curve σ_k satisfied the relationship

$$\sigma_k > 10^{-10} f, \text{ (f = frequency in cps)} \tag{46}$$

then the device may be described by a group B model. If it does not satisfy that relationship, more information is required to determine which group of models apply. Simpler criteria exist if the dielectric thickness L and the absorption coefficient α are known. Group A applies if $\alpha L > 1$, and group B if $\alpha L < 1$. For the CdS photocapacitor data plotted in Figure 13 the inequality for σ_k is satisfied by an order of magnitude so the model must be determined from group B.

The second step is to determine the variation of conductivity with light intensity. For the group B models the equivalent conductivity and the conductivity are identical; therefore, the parameter β is determined from the slope of the experimental data plotted in Figure 17. In this case $\beta = 1/2$, and the equations describing the model are

$$\sigma = \sigma_{eq} = p_\sigma \phi^{1/2} \tag{47}$$

and

$$\varepsilon = \varepsilon_o \varepsilon_r + p_\varepsilon \phi^{\delta} \tag{48}$$

where no assumptions are made concerning the parameter δ. Equation 48 may be rewritten

$$C/C_o = 1 + p_\varepsilon \phi^\delta / \varepsilon_o \varepsilon_r . \tag{49}$$

The following definitions are made to solve for the value of δ that results in the least-mean-square-error fit for the model:

$$I = \log(C/C_o - 1), \tag{50}$$

$$R = \log(\sigma_{eq}), \tag{51}$$

also I_i and R_i are the i-th set of experimental data and i = 1,2,...k. By definition, the mean-square-error is

$$E = \frac{1}{k} \sum_{i=1}^{k} (I - I_i)^2 \tag{52}$$

with $R = R_i$. Light intensity ϕ is eliminated by combining Equations 47 and 49 to yield

$$C/C_o - 1 = \frac{p_\varepsilon}{\varepsilon_o \varepsilon_r} \left(\frac{\sigma_{eq}}{p_\sigma}\right)^{2\delta}. \tag{53}$$

If a new parameter is defined as

$$b = \log[p_\varepsilon / \varepsilon_o \varepsilon_r (p_\sigma)^{2\delta}], \tag{54}$$

then $$I = b + 2\delta R. \tag{55}$$

The least-mean-square-error is determined by setting the partial derivatives equal to zero, i.e.,

$$\frac{\partial E}{\partial \delta} = \frac{\partial E}{\partial b} = 0. \tag{56}$$

Differentiating Equation 52 with respect to b results in

$$\frac{\partial}{\partial b} \sum_{i=1}^{k} (I - I_i)^2 = \sum_{i=1}^{k} \frac{\partial}{\partial b} (b + 2\delta R_i - I_i)^2 = 0.$$

Consequently

$$bk + 2\delta \sum_{i=1}^{k} R_i = \sum_{i=1}^{k} I_i. \tag{57}$$

Minimizing with respect to δ yields

$$b \sum_{i=1}^{k} R_i + 2\delta \sum_{i=1}^{k} (R_i)^2 = \sum_{i=1}^{k} (R_i)(I_i). \tag{58}$$

The parameters δ and b are determined in terms of experimental data by solving Equations 57 and 58,

$$\delta = (\frac{1}{2}) \frac{k \sum_{i=1}^{k} (R_i)(I_i) - [\sum_{i=1}^{k} R_i][\sum_{i=1}^{k} I_i]}{k \sum_{i=1}^{k} (R_i)^2 - [\sum_{i=1}^{k} R_i]^2} \tag{59}$$

$$b = \frac{[\sum_{i=1}^{k} I_i][\sum_{i=1}^{k} (R_i)^2] - [\sum_{i=1}^{k} R_2][\sum_{i=1}^{k} (R_i)(I_i)]}{k \sum_{i=1}^{k} (R_i)^2 - [\sum_{i=1}^{k} R_i]^2}. \tag{60}$$

Using six experimental data with f = 1 Mcs. yields $\delta \doteq 1$. This value agrees with the original assumption for the variation of permittivity with light intensity. Using the same data to determine b yields

$$b = -0.6.$$

Substituting the results for δ and b into Equation 53 yields

$$C/C_o = 1 + 0.25(\sigma_{eq})^2 .10^6. \tag{61}$$

This equation is plotted in Figure 15 together with experimental data for f = 1.0 Mcs. The good fit indicates that group B, with the parameters $\beta = 1/2$ and $\delta = 1$, represents the CdS photocapacitor very well.

If the model is an accurate representation of the actual physical processes occurring within the crystal, then certain conclusions may be drawn. The fact that a model from group B was required indicates $\alpha L < 1$ or the absorption coefficient α is less than 15 cm^{-1}. The variation of conductivity as the square root of light intensity is theoretically due to either a trap-free material or a material with more electrons in deep traps than shallow traps (3, 25). The experimental data for the CdS photocapacitor plotted in Figure 14 indicates that the latter is true. Figure 14 is a plot of the transient in a.c. conductance and capacitance due to removing the illumination. The relatively slow change in both capacitance and conductance is due to the emptying of the traps by thermal excitation. The carriers remain trapped for a finite length of time but without optical generation they are not replenished and hence the decay of permittivity to the dark value. The conductance transient is due to the

fact that the majority of the carriers enter into the conduction process upon leaving the traps until recombination occurs.

A complete theoretical analysis of the dependence of permittivity on light intensity has not been made. A study of the variation of both conductivity and permittivity with light intensity should include an analysis of the polarizability of carriers at various trapping and recombination levels and an analysis of the density of the occupied levels as a function of light intensity. A useful experiment to complement such a study would be to correlate the photo-induced changes in conductivity and permittivity with the wavelength of the optical excitation. The spectrum should include wavelengths in the absorption region as well as wavelengths greater than the absorption edge to obtain the most information about the contribution of traps and recombination centers. Wide band illumination was used for the experiments reported in this investigation and; therefore, no conclusions can be made concerning the various wavelengths.

The models proposed in this dissertation should help in the interpretation of results from other materials, from thicker devices, and for other distributions of defect states in the forbidden region. The main purpose of the models is to correlate theory and experimental results.

APPENDIX

Digital Computer Programs

Several digital computer programs were written for the Iowa State University Cyclone Computer to determine the equivalent conductivity σ_{eq} and the normalized capacitance C/C_o for the photocapacitor models in group A. In terms of the real and imaginary parts of the normalized admittance y,

$$C/C_o = (\text{imaginary part of } y)/\varepsilon_o \varepsilon_r \omega$$

and $$\sigma_{eq} = (\text{real part of } y)$$

The symbols are all defined in Table 1. Three equations are derived in the chapter on Mathematical Models that define the normalized admittance for the four models in group A.

For models 1 and 2

$$y = \frac{\gamma(y_o - y_i)^{1/2}(y_o + y_i)^{1/2}}{\ln \dfrac{(y_o + y_i)^{1/2} + (y_o - y_i)^{1/2} \tanh(\gamma/2)}{(y_o + y_i)^{1/2} - (y_o - y_i)^{1/2} \tanh(\gamma/2)}}$$

where $y_o = \sigma_o + j\omega\varepsilon_o\varepsilon_r$ and $y_i = (p_\sigma + j\omega p_\varepsilon)2\phi_o e^{-\gamma}$ with $p_\varepsilon = o$ for model 1 and $p_\varepsilon \neq o$ for model 2.

The normalized admittance for model 3 is

$$y = \frac{\gamma y_o}{\ln \frac{e^{\gamma} y_o + y_i'}{y_o + y_i'}}$$

where $y_o = \sigma_o + j\omega\epsilon_o\epsilon_r$ and $y_i' = (p_\sigma + j\omega p_\epsilon)\phi_o$.

For model 4, if $q = \omega^2 p_\epsilon^2 + 4j\omega\epsilon_o\epsilon_\gamma p_\sigma$ then

$$\frac{1}{y} = \frac{-1}{2j\omega\epsilon_o\epsilon_r\alpha}\left[-2\gamma + \ln \frac{p_\sigma\phi_o^2 + j\omega p_\epsilon\phi_o + j\omega\epsilon_o\epsilon_r}{p_\sigma\phi_o^2 e^{-2\gamma} + j\omega p_\epsilon\phi_o e^{-\gamma} + j\omega\epsilon_o\epsilon_r}\right.$$

$$\left. \frac{-\omega p_\epsilon}{q} \ln \frac{(2p_\sigma\phi_o e^{-\gamma} + j\omega p_\epsilon - jq)(2p_\sigma\phi_o + j\omega p_\epsilon + jq)}{(2p_\sigma\phi_o e^{-\gamma} + j\omega p_\epsilon + jq)(2p_\sigma\phi_o + j\omega p_\epsilon - jq)}\right].$$

Three Fortran programs were written to solve the foregoing equations. Several modifications and additions were made to each of these to obtain the results in different forms. For example, an auxiliary program was written to determine the optimum values of γ, p_σ, p_ϵ and ϵ_r for a least-mean-square-error fit between experimental results and model 4.

Several operations are required to compute y because the computer will not solve problems involving complex numbers. For example, the subroutine to multiply two complex numbers must determine the magnitude and angle associated with each number and then multiply the magnitudes together and add the angles. Checks must also be made to insure that division by zero is not permitted and to determine what quadrant the angles are in. Subroutines were also written to add, take the square root

and find the natural logarithm of a complex number.

Input data to a program consisted of σ_o, f, ε_o, γ, p_σ, p_ε, and ϕ_o. To obtain a curve of C/C_o versus σ_{eq} one or more of the input parameters was increased by multiplying factors that were part of the input data. A maximum range for both the parameters and the output results were also included with the input data and the limits were checked in the programs.

Figure 18 is a Fortran flow-chart for computing the equivalent conductivity and the normalized capacitance for models 1 and 2, group A. Each complete program requires several typewritten pages so they are not included.

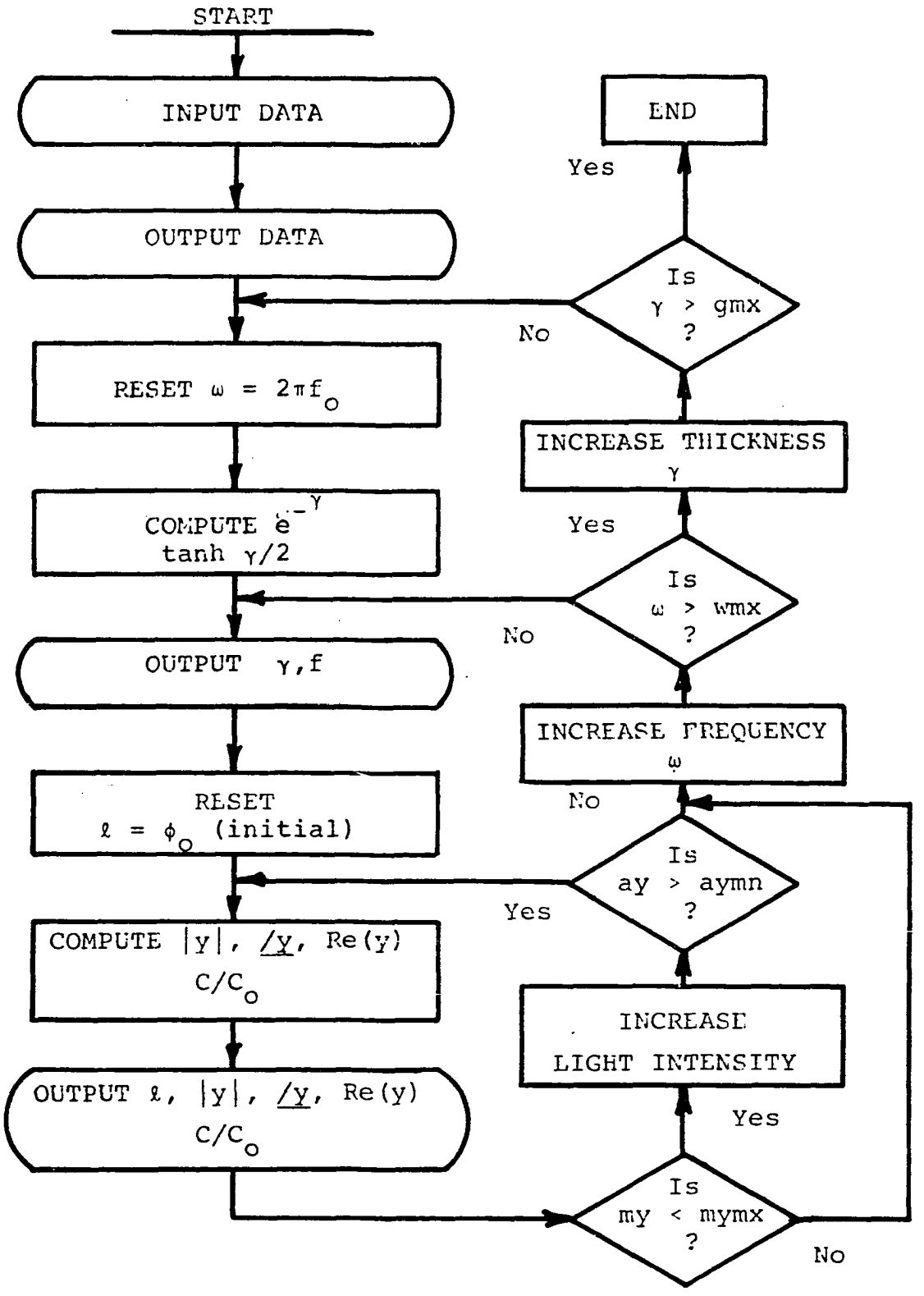

Figure 18. Flow chart for Fortran Program to compute equivalent conductivity and normalized capacitance at different light intensities, frequencies, thicknesses and optical sensitivity parameters

BIBLIOGRAPHY

1. Berlincourt, Don, Hans Joffe and L. R. Shiozawa. Electroelastic properties of the sulfides, selenides, and tellurides of zinc and cadmium. Physical Review 129:1009-1017. 1963.

2. Bube, R. H. Photoconductivity of the sulfide, selenide and telluride of zinc or cadmium. Proceedings of the IRE 43:1836-1850. 1955.

3. Bube, Richard H. Photoconductivity of solids. John Wiley and Sons, Inc., New York, N. Y. 1960.

4. Ehret, Dorris M. Photoconductivity of cadmium sulfide. Unpublished M.S. thesis. Ames, Iowa, Library, Iowa State University of Science and Technology. 1949.

5. Frederikse, H. P. R. and R. F. Blunt. Photoeffects in intermetallic compounds. Proceedings of the IRE 43:1828-1835. 1955.

6. Garlick, G. F. J. Absorption, emission and storage of energy in phosphors. British Journal of Applied Physics Supplement 4:S85-S88. 1955.

7. Garlick, G. F. J. The electrical properties of phosphors. Alan F. Gibson, general editor. Progress in semiconductors Vol. 1. pp. 101-133. John Wiley and Sons, Inc., New York, N. Y. 1956.

8. Garlick, G. F. J. and A. F. Gibson. Dielectric changes in phosphors containing more than one activator. Proceedings of the Physical Society of London. 62, Part 2:731-736. 1949.

9. Garlick, G. F. J. and A. F. Gibson. Electron traps and dielectric changes in phosphorescent solids. Proceedings Royal Society of London Series A, 188:485-509. 1947.

10. Goodman, Alvin M. Evaporated metallic contacts to conducting cadmium sulfide single crystals. Journal of Applied Physics 35:573-580. 1964.

11. Gordon, F., Jr., P. Newman, Jr., J. Handen and H. Jacobs. Cadmium sulfide photocapacitor. Institute of Radio Engineers National Convention Record 1957, Part 3:40-48. 1957.

12. Holland, L. Vacuum deposition of thin films. Chapman and Hall Limited, London. 1963.

13. Ioffe, A. F. Physics of semiconductors. Academic Press, Inc., New York, N. Y. 1960.

14. Kallmann, Hartmut and Bernard Kramer. Calculation of the photoconductivity from A.C. impedance changes induced in ZmS and ZmCdS phosphors. J. Phys. Chem. Solids 10:59-63. 1959.

15. Kallmann, Hartmut, Bernard Kramer and Peter Mark. Impedance measurements on CdS crystals. Physical Review 99:1328-1331. 1955.

16. Kallmann, Hartmut, Bernard Kramer and Arnold Perlmutter. Induced conductivity in luminescent powders. II. AC impedance measurements. Physical Review 89:700-707. 1953.

17. Karakushan, E. I. and V. I. Stafeev. Large area magnetodiodes. Soviet Physics-Solid State 3:1476-1482. 1962.

18. Karakushan, E. I. and V. I. Stafeev. Magnetodiodes. Soviet Physics-Solid State 3:493-498. 1961.

19. Kronenberg, Stanley and Carl A. Accardo. Dielectric changes in inorganic phosphors. Physical Review 107:989-992. 1956.

20. Mark, Peter and Hartmut P. Kallmann. AC impedance measurements of photoconductors containing blocking layers analysed by the Maxwell-Wagner theory. J. Phys. Chem. Solids 23:1067-1078. 1962.

21. Moss, T. S. Optical properties of semiconductors. Butterworths Scientific Publications, London, England. 1959.

22. Oksman, Ya A., M. N. Kiseleva and B. M. Martinson. Drift dispersion of the photocapacitance effect in doped germanium. Soviet Physics-Solid State 5:159-161. 1963.

23. Rook, H. L. and R. C. Plumb. The tungsten content of aluminum films evaporated from tungsten heaters. Applied Physics Letters 1: 11-12. 1962.

24. Rose, A. An outline of some photoconductive processes. RCA Review 12:362-414. 1951.

25. Rose, Albert. Concepts in photoconductivity and allied problems. Interscience Publishers, a division of John Wiley and Sons, New York, N. Y. 1963.

26. Rose, Albert. Performance of photoconductors. Proceedings of the IRE 43:1850-1869. 1955.

27. Sihvonen, Y. T. and D. R. Boyd. Transparent indium contacts to CdS. The Review of Scientific Instruments 31:992-994. 1960.

28. Sihvonen, Y. T. and D. R. Boyd. Analysis and performance of a light-sensitive capacitor. Proceedings of the IEEE 53:378-385. 1965.

29. Smith, R. W. Properties of ohmic contacts to cadmium sulfide single crystals. Physical Review 97:1525-1530. 1955.

30. Smith, R. W. Some aspects of the photoconductivity of cadmium sulfide. R.C.A. Review 12:350-361. 1951.

31. Stafeev, V. I. Modulation of diffusion length as a new principle of operation of semiconductor devices. Soviet Physics-Solid State 1:763-768. 1959.

32. Weimer, Paul K. The TFT - a new thin film transistor. Proceedings of the IRE 50:1462-1469. 1962.

ACKNOWLEDGEMENTS

The author wishes to express his appreciation to Dr. G. G. Koerber for his help and guidance throughout the research and to Dr. R. C. Camp and Prof. R. A. Sharpe for their assistance in writing the digital computer programs. Digital computing time was furnished by the Iowa State University Cyclone Computer Laboratory. Valuable technical assistance was obtained from Mr. D. H. Grotzky and Mr. D. L. Anderson of the Ames Laboratory of Atomic Energy Commission in orientation and cutting the cadmium sulfide crystal. Financial support for this investigation was primarily from the Industrial Affiliate program in Solid State Electronics at Iowa State University. The author also appreciates the time allotted by the University of Missouri at Rolla to complete this paper.